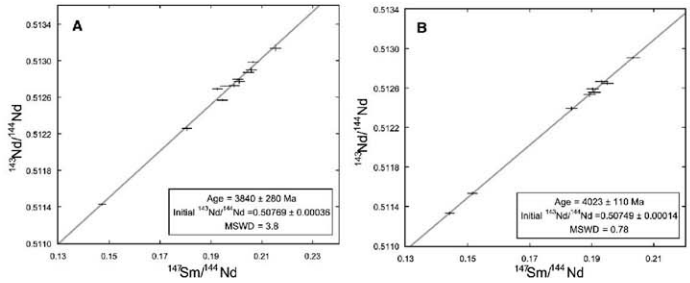

Fig. 4. ^{147}Sm-^{143}Nd isochron diagrams. **(A)** Ultramafic to gabbroic samples from one differentiated sill. **(B)** Samples from the gabbro sills that show a strong gneissic metamorphic texture.

perhaps not as depleted as suggested by the Greenland data (*7*, *17*, *19*). As a result, the calculated ^{143}Nd depleted-mantle model ages (T_{DM}) for the faux-amphibolite, except PC-129, range from 4.1 to 4.4 Ga, consistent with the age suggested by ^{142}Nd systematics and in contrast to the 3.2 to 3.6 Ga T_{DM} values of the gabbros and sample PC-129 (table S2).

Whether or not the faux-amphibolite is 4.28 Gy old, its compositional characteristics may provide clues to the process of crust formation in the Hadean (>4.0 Ga). The basaltic major and compatible (e.g., Ni) trace element composition of the faux-amphibolite is consistent with derivation from a peridotitic mantle. Compared to the gabbros and to modern mid-ocean ridge basalts, the most unusual compositional characteristic of the faux-amphibolite is its low Ca content, high K and Rb contents, and LREE enrichment. Because elements like K and Rb are easily affected by alteration, however, it is unclear whether these are magmatic features of the faux-amphibolite. The LREE enrichment could reflect relatively low degrees of mantle melting, but this explanation is not supported by the relatively low concentration of elements such as Ti and Nb in the faux-amphibolite. The high LREE to Nb ratios of the faux amphibolite, however, is similar to that of modern calc-alkaline melts produced in convergent margin settings. The Hadean crust, represented by the faux-amphibolite, was intruded at 4.0 and 3.8 Ga by gabbro and ultramafic sills that have the ^{143}Nd and ^{142}Nd isotopic composition of the depleted mantle at the time of their intrusion. The low $^{142}Nd/^{144}Nd$ ratios of tonalites and felsic bands that were emplaced between 3.8 and 3.6 Ga, well after ^{146}Sm was extinct (*9*–*11*), suggest that they formed by the partial melting of the faux-amphibolite.

References and Notes

1. S. A. Bowring, I. S. Williams, *Contrib. Mineral. Petrol.* **134**, 3 (1999).
2. S. A. Wilde, J. W. Valley, W. H. Peck, C. M. Graham, *Nature* **409**, 175 (2001).
3. M. Boyet *et al.*, *Earth Planet. Sci. Lett.* **214**, 427 (2003).
4. G. Caro, B. Bourdon, J. Birck, S. Moorbath, *Nature* **423**, 428 (2003).
5. M. Boyet, R. W. Carlson, *Earth Planet. Sci. Lett.* **250**, 254 (2006).
6. G. Caro, B. Bourdon, J. Birck, S. Moorbath, *Geochim. Cosmochim. Acta* **70**, 164 (2006).
7. V. C. Bennett, A. D. Brandon, A. P. Nutman, *Science* **318**, 1907 (2007).
8. J. O'Neil *et al.*, in *In Earth's Oldest Rocks*, M. van Kranendonk, R. H. Smithies, V. C. Bennett, Eds. (Elsevier, Amsterdam, 2007), pp. 219–250.
9. J. David, L. Godin, R. K. Stevenson, J. O'Neil, D. Francis, *Geol. Soc. Am. Bull.*, in press (available at www.gsajournals.org/perlserv/?request=get-abstract&doi=10.1130%2FB26369.1).
10. M. Simard, M. Parent, J. David, K. N. M. Sharma, "Géologie de la région de la rivière Innuksuac (34K et 34L)" (Ministère des Ressources naturelles, RG 2002-10, Québec, Canada, 2003).
11. N. L. Cates, S. J. Mojzsis, *Earth Planet. Sci. Lett.* **255**, 9 (2007).
12. M. Boyet, R. W. Carlson, *Science* **309**, 576 (2005); published online 16 June 2005 (10.1126/science.1113634).
13. G. W. Lugmair, S. J. G. Galer, *Geochim. Cosmochim. Acta* **56**, 1673 (1992).
14. Y. Amelin, A. N. Krot, I. D. Hutcheon, A. A. Ulyanov, *Science* **297**, 1678 (2002).
15. D. J. DePaolo, *Nature* **291**, 193 (1981).
16. S. L. Goldstein, R. K. O'Nions, P. J. Hamilton, *Earth Planet. Sci. Lett.* **70**, 221 (1984).
17. V. C. Bennett, A. P. Nutman, M. T. McCulloch, *Earth Planet. Sci. Lett.* **119**, 299 (1993).
18. M. T. McCulloch, V. C. Bennett, *Geochim. Cosmochim. Acta* **58**, 4717 (1994).
19. M. T. McCulloch, V. C. Bennett, in *The Earth's Mantle*, I. Jackson, Ed. (Cambridge Univ. Press, Cambridge, 1998), pp. 127–158.

20. This research was supported by National Science and Engineering Research Council of Canada (NSERC) Discovery grants to D.F. (RGPIN 7977-00). We thank the municipality of Inukjuak and the Pituvik Landholding Corporation for permission to work on their territory; J. Mina, M. Carroll, V. Inukpuk Morkill, R. Kasudluak, and J. Williams for their hospitality and support; and M. Horan and T. Mock for analytical support. The Department of Terrestrial Magnetism Thermo-Fisher Scientific Triton (Bremen, Germany) was purchased with partial support from the NSF grant EAR-0320589.

Supporting Online Material

www.sciencemag.org/cgi/content/full/321/5897/1828/DC1
Materials and Methods
Tables S1 to S6
Figs. S1 and S2
References

17 June 2008; accepted 19 August 2008
10.1126/science.1161925

Infants' Perseverative Search Errors Are Induced by Pragmatic Misinterpretation

József Topál,[1]* György Gergely,[1,2] Ádám Miklósi,[3] Ágnes Erdőhegyi,[3] Gergely Csibra[2,4]

Having repeatedly retrieved an object from a location, human infants tend to search the same place even when they observe the object being hidden at another location. This perseverative error is usually explained by infants' inability to inhibit a previously rewarded search response or to recall the new location. We show that the tendency to commit this error is substantially reduced (from 81 to 41%) when the object is hidden in front of 10-month-old infants without the experimenter using the communicative cues that normally accompany object hiding in this task. We suggest that this improvement is due to an interpretive bias that normally helps infants learn from demonstrations but misleads them in the context of a hiding game. Our finding provides an alternative theoretical perspective on the nature of infants' perseverative search errors.

Human infants' abilities for understanding the physical world are often tested in hide-and-search tasks. First demonstrated by Piaget (*1*), the perseverative search error (sometimes called the A-not-B error) is a well-known and robust mistake that infants close to 1 year of age normally commit. In the standard A-not-B task, a demonstrator repeatedly places an object

under one (A) of two opaque containers (A and B) in full view of the infant. After each hiding event, the infant is allowed to retrieve the object. This is followed by test trials where the demonstrator places the object under container B and allows the infant to search for it. Despite just having seen the object being hidden at the new B location, infants between 8 and 12 months of age frequently look for it under container A where it had been previously hidden. This perseverative search error continues to be of theoretical interest for researchers of cognitive development (*2*–*6*).

A wide range of explanations have been proposed to account for this response bias. According to Piaget's original hypothesis (*1*), the A-not-B error reflects young infants' as yet incomplete comprehension of object permanence. Piaget believed that the infant conceives the appearance of the object under container A to be an inherent consequence of the search response itself. More recent accounts of the perseverative bias have focused on the motor response involved in searching at location A, which has been primed during its repeated execution after the initial hiding trials. In these accounts, the A-not-B error is usually ascribed to a deficit in inhibitory control over a previously rewarded motor response (*7*) or to constraints on short-term memory (*8*), or both (*9*). Alternatively, the perseverative response has been seen as driven by a response bias established in the visuomotor response execution system during repeated A-trials (*10*). Others point out that simply observing another person reaching to location A repeatedly is in itself sufficient to elicit the A-not-B error. In this view, infants' errors do not reflect their difficulty with response inhibition, but are due to an attentional bias to the location where the previously observed manual responses have been directed (*11*). A more recent explanation suggests that observing repeated hiding events at location A leads to automatic motor simulation (covert imitation) of the action through the activation of the mirror neuron system (*12*).

In contrast to the focus of such accounts on infants' repeated responses directed at container A, we have examined the perseverative error from a different perspective by exploring the potential role of the communicative demonstration context of the task. The A-not-B task normally involves face-to-face interaction, in which object hiding is accompanied by the demonstrator's ostensive and referential signals [such as eye contact, infant-directed speech, addressing the baby by name, and pointing at and/or looking back and forth between the hiding location and the infant (*13*)]. Recent findings indicate that ostensive-referential communicative signals can play an interpretation-modulating role, leading to selective encoding of different aspects of action demonstrations in social learning tasks [e.g., (*14*–*17*)]. Csibra and Gergely (*13*, *18*) hypothesized that ostensive signals induce a receptive "pedagogical learning stance" in the infant, involving a built-in interpretive bias of generalizability. This bias assumes that ostensively communicated manifestations are more likely to convey semantic or generic information about the referent than episodic information that obtains only in the here-and-now.

The hiding events in the standard A-not-B task can be interpreted both as indicating episodic information about the referent's current location ("the target object is now under container A") and as communicating information about some generalizable property of the referent kind (e.g., "this type of object is usually found in container A"). We hypothesized that in the A-not-B paradigm, the interpretive bias of generalizability may result in a pragmatic misinterpretation of the object-hiding actions as potential teaching demonstrations. As a result, the infant would tend to infer and learn some generalizable information, such as "this kind of object is to be found in container A" or "we keep toys in container A." According to this hypothesis, misinterpretation of the ostensively communicated hiding events leads infants to commit the perseverative search error during B test trials. We therefore predicted that in a noncommunicative action observation condition, which lacks ostensive signals but provides experience with repeated motor search responses directed at container A, the perseverative search error should be reduced.

To test this hypothesis, we examined infants' object search behavior in the A-not-B task while varying the presence or absence of the social-communicative context of the hiding events. Three groups of 10-month-old infants (14 in each) were tested. In the ostensive-communicative context (OC) (Fig. 1A), the demonstrator established eye contact with the baby, smiling at and addressing him or her in infant-directed speech (saying "Hello baby, look here!"). Then she repeatedly hid a toy object under container A while shifting her eye gaze back and forth between the infant and the container to direct and share the infant's attention toward the object-hiding action. In the noncommunicative context (NC) (Fig. 1B), the demonstrator's face and torso were oriented 90° away from the infant and, while her hands were just as visible during the repeated hiding actions as in the OC condition, she never looked at or communicated with the infant in any way while hiding the object. In the nonsocial context (NS) (Fig. 1C), the demonstrator acted from behind a curtain and only the object's movements were visible to the infant. In each condition, after a 4-s delay following the hiding events, the demonstrator slid the cardboard sheet with the two containers closer to the infant and then waited until a search response was executed. The toy was hidden four times at the first location (A-trials), then three times at the other location (B-trials) (*19*).

We analyzed the proportion of correct responses in both the A- and B-trials, as well as the

[1]Research Institute for Psychology, Hungarian Academy of Sciences, Budapest H-1132, Hungary. [2]Department of Philosophy, Central European University, Budapest H-1051, Hungary. [3]Department of Ethology, Eötvös University, Budapest H-1117, Hungary. [4]School of Psychology, Birkbeck, University of London, London WC1 E7HX, UK.

*To whom correspondence should be addressed. E-mail: topaljozsef@gmail.com

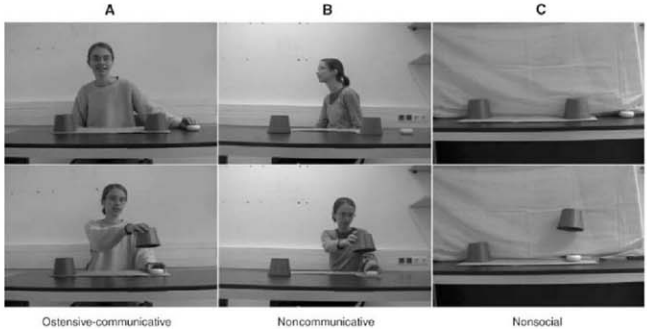

Fig. 1. Experimental arrangement in the three hiding contexts: **(A)** ostensive-communicative task, **(B)** noncommunicative task, and **(C)** nonsocial task.

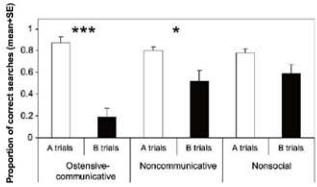

Fig. 2. Proportion of correct searches (mean + SE) in A- and B-trials as a function of the hiding context. The 10-month-old infants received four A-trials followed by three B-trials. ***$P < 0.0001$, *$P < 0.05$.

Table 1. Number of infants in the three different hiding contexts (14 in each group) committing at most one or more search errors (searching at location A) in the three B-trials.

Context	0 or 1 error	2 or 3 errors
Ostensive-communicative	2	12
Noncommunicative	8	6
Nonsocial	9	5

number of infants who committed the A-not-B error (searched more than once at location A in the B-trials) as a function of the hiding context. We found that the magnitude of the A-not-B error was considerably smaller in the noncommunicative and nonsocial conditions than in the traditional ostensive-communicative context (Fig. 2 and fig. S1). A two-way analysis of variance on the proportion of correct responses, with phase (A- versus B-trials) and hiding context (OC, NC, NS) as factors, showed more correct responses in the A-trials than in the B-trials ($F_{1,39} = 49.376$, $P < 0.0001$) and a significant interaction between these factors ($F_{2,39} = 8.041$, $P = 0.001$). This interaction was because the change of the proportion of correct searches from the A- to the B-trials differed across contexts. Whereas in the OC context the initial success rate of 0.88 in the A-trials dropped to 0.19 in the B-trials ($t_{13} = 8.917$, $P < 0.0001$), the drop was much smaller in the NC context (0.80 to 0.52, $t_{13} = 2.536$, $P = 0.025$) and was not statistically significant in the NS context (0.78 to 0.59, $t_{13} = 1.96$, $P = 0.072$). In addition, although the infants were similarly successful during the A-trials in all contexts ($F_{2,39} = 1.525$, $P = 0.23$), their search performance differed significantly across contexts in the B-trials ($F_{2,39} = 6.660$, $P = 0.005$). In this latter case, post hoc pairwise comparisons (Tukey-Cramer test) showed that infants searched the least correctly in the OC context (OC versus NO, $P < 0.05$; OC versus NS, $P < 0.01$).

Comparison of the number of infants committing the A-not-B error (Table 1) indicated a significant difference between demonstration conditions ($\chi^2 = 8.265$, $P = 0.016$). After having witnessed ostensive-communicative hiding demonstrations during the A-trials, 86% of the infants displayed the perseverative error during the B-trials. In contrast, the majority of infants in the other two contexts (NC, 57%; NS, 64%) did not show a perseverative response pattern.

These results are not compatible with the currently widely accepted explanations for the A-not-B perseverative response bias, which attribute this robust developmental phenomenon to the dominance (and lack of inhibition) of the prepotent motor search response. Our results also challenge recent proposals that the motor priming of the prepotent response can be induced by simply observing the manual hiding actions directed at location A, mediated by the mirror neuron system (*12*), because the NC and OC contexts provided the same amount of visual (as well as motor) experience of the repeated manual hiding actions directed at container A.

Rather, we suggest that our results can be explained by the theory of natural pedagogy (*13*, *14*), which proposes a special interpretation-modulating role for ostensive-referential signals in early social learning. The action demonstrations of the A-not-B paradigm can be interpreted either as a hide-and-search game, presenting the infant with episodic (here-and-now) information about the whereabouts of the object (correct interpretation), or as a kind of teaching session that conveys generalizable information about properties of the objects (toys or containers) for the infant to learn (incorrect interpretation). We propose that it is this latter kind of interpretation—mistakenly established during the ostensively demonstrated A-trials—that remains dominant during the B-trials, leading to the erroneous perseverative search responses.

This conclusion does not invalidate the contribution of other cognitive factors to the A-not-B error identified by earlier studies. In our study, the perseverative error was reduced but did not completely disappear in the NC and NS contexts, which suggests that infants' search behavior also depends on their inhibitory, information processing, and memory skills (*20*–*21*). Had we not inserted a 4-s delay between hiding and searching, infants would have been likely to search for the toy at the correct location (*22*, *23*). Thus, the decay of the accessibility of the short-term memory of target location for search actions is a necessary component of the search error. Similarly, the ostensive hiding demonstration may have generated higher cognitive load to be overcome in search behavior than did the NC and NS contexts (*22*). Although these accounts could explain why infants did not search at the correct location, they predict random search rather than perseveration. However, it was only in the NS and NC conditions that infants' search pattern was close to 50%; in the OC condition, they tended to search more often at location A. The theory of natural pedagogy offers an explanation for this baffling tendency to perseverate: The communicative demonstration during the A-trials generates a semantic (and potentially long-term) memory trace that biases infants to search at the old location when they no longer have access to the decayed memory trace of the current location or when their information-processing capacity is overloaded. In addition, the primacy effect of semantic learning (as opposed to the recency effect on episodic memory) made it difficult for the infants to relearn the new location in B-trials.

Human infants are highly social creatures (*24*) who cannot help but interpret the ostensive communicative signals directed to them. Although such a disposition prepares them to efficiently learn from adults, in certain situations (e.g., the A-not-B task) it can also misguide their performance. Our demonstration of the social communicative determinants of infants' early tendency for perseveration in motor search tasks provides independent support for our general proposal (*13*) that sensitivity to ostensive-referential communication is a basic evolutionary adaptation that is fundamental to the emergence of human social cognition.

References and Notes

1. J. Piaget, *The Construction of Reality in the Child* (Basic Books, New York, 1954).
2. P. L. Harris, in *Infant Development*, A. Slater, G. Bremner, Eds. (Erlbaum, Hove, UK, 1989), pp. 103–122.
3. H. M. Wellmann, D. Cross, K. Bartsch, *Monogr. Soc. Res. Child Dev.* **51**, 3 (1986).
4. S. Marcovitch, P. D. Zelazo, *Child Dev.* **70**, 1297 (1999).
5. E. Thelen, G. Schöner, C. Scheier, L. B. Smith, *Behav. Brain Sci.* **24**, 1 (2001).
6. T. Ruffman, L. Slade, J. C. Sandino, A. Fletcher, *Child Dev.* **76**, 122 (2005).
7. A. Diamond, *Child Dev.* **56**, 868 (1985).
8. E. M. Cummings, E. L. Bjork, *Mem. Cognit.* **12**, 1 (1984).
9. A. Diamond, L. Cruttenden, D. Neiderman, *Dev. Psychol.* **30**, 192 (1994).
10. L. B. Smith, E. Thelen, R. Titzer, D. McLin, *Psychol. Rev.* **106**, 235 (1999).
11. T. Ruffman, L. Langman, *Infant Behav. Dev.* **25**, 237 (2002).
12. M. R. Longo, B. I. Berthental, *Infancy* **10**, 43 (2006).
13. G. Csibra, G. Gergely, in *Processes of Change in Brain and Cognitive Development*, Y. Munakata, M. Johnson, Eds. (Oxford Univ. Press, Oxford, 2006), pp. 249–274.
14. G. Gergely, K. Egyed, I. Király, *Dev. Sci.* **10**, 139 (2007).
15. A. Brugger, L. A. Lariviere, D. L. Mumme, E. W. Bushnell, *Child Dev.* **78**, 806 (2007).
16. M. Nielsen, *Dev. Psychol.* **42**, 555 (2006).
17. Y. M. D. Yoon, M. H. Johnson, G. Csibra, *Proc. Natl. Acad. Sci. U.S.A.* **105**, 13690 (2008).
18. G. Gergely, G. Csibra, in *Roots of Human Sociality: Culture, Cognition, and Human Interaction*, N. J. Enfield, S. C. Levinson, Eds. (Berg, Oxford, 2006), pp. 229–255.
19. See supporting material on *Science* Online.
20. A. Diamond, *Ann. N.Y. Acad. Sci.* **608**, 267 (1990).
21. R. Keen, R. L. Caricco, M. R. Sylvia, N. E. Berthier, *Dev. Sci.* **6**, 221 (2003).
22. A. Diamond, P. S. Goldman-Rakic, *Exp. Brain Res.* **74**, 24 (1989).
23. A. Ahmed, T. Ruffman, *Dev. Psychol.* **34**, 441 (1998).

24. E. Herrmann, J. Call, M. V. Hernández-Loreda, B. Hare, M. Tomasello, *Science* **317**, 1360 (2007).
25. We thank J. Bognár for her assistance in data collection, and V. Southgate and J. Watson for helpful comments. Supported by the Hungarian Scientific Research Fund (T049615), the EU6 Framework Programme (NEUROCOM grant 12738, EDICI grant 12929), and the Bolyai Foundation of the Hungarian Academy of Sciences.

Supporting Online Material
www.sciencemag.org/cgi/content/full/321/5897/1831/DC1
Materials and Methods
SOM Text
Fig. S1
Tables S1 and S2

5 June 2008; accepted 28 August 2008
10.1126/science.1161437

Antigen Recognition by Variable Lymphocyte Receptors

Byung Woo Han,[1,2] Brantley R. Herrin,[3] Max D. Cooper,[3] Ian A. Wilson[1,2]*

Variable lymphocyte receptors (VLRs) rather than antibodies play the primary role in recognition of antigens in the adaptive immune system of jawless vertebrates. Combinatorial assembly of leucine-rich repeat (LRR) gene segments achieves the required repertoire for antigen recognition. We have determined a crystal structure for a VLR-antigen complex, VLR RBC36 in complex with the H-antigen trisaccharide from human blood type O erythrocytes, at 1.67 angstrom resolution. RBC36 binds the H-trisaccharide on the concave surface of the LRR modules of the solenoid structure where three key hydrophilic residues, multiple van der Waals interactions, and the highly variable insert of the carboxyl-terminal LRR module determine antigen recognition and specificity. The concave surface assembled from the most highly variable regions of the LRRs, along with diversity in the sequence and length of the highly variable insert, can account for the recognition of diverse antigens by VLRs.

In the lamprey and hagfish, the only surviving jawless vertebrates, variable lymphocyte receptors (VLRs) play the major role in recognition of foreign antigens (*1*, *2*). In contrast to the variable, diverse, and joining gene segments (VDJs) of immunoglobulins in jawed vertebrates, the jawless vertebrates have solved the receptor diversity problem by somatic DNA rearrangement of diverse leucine-rich repeat (LRR) modules into incomplete *vlr* genes. The resulting mature *vlr* genes encode an N-terminal LRR capping region (LRRNT), the first LRR (LRR1), up to seven 24-residue variable LRRs (LRRVs) (*3*), a terminal or end LRRV (LRRVe), a connecting peptide (CP), a C-terminal LRR capping region (LRRCT), and a threonine/proline-rich stalk region that connects the protein to a glycosylphosphatidylinositol (GPI) anchor and a hydrophobic tail (Fig. 1A) (*1*, *2*, *4*).

From these somatic gene rearrangements, a potential repertoire of about 10^{14} unique VLRs has been estimated (*2*), which compares favorably with the equivalent diversity attainable through VDJ recombination in antibodies. Different numbers and combinations of LRR modules, coupled with amino acid sequence variation in the LRR segments, thereby contribute to VLR diversity. The LRR repeats form a curved solenoid, as in Toll-like receptors (TLRs) (*5*, *6*), and its concave surface has been suggested as the antigen-binding site from evolutionary, sequence, and mutational analyses (*2*, *7*, *8*). Crystal structures of three unliganded hagfish VLRs with different numbers of LRRV modules have been determined (*7*), whereas antigen-binding specificity [erythrocyte H-trisaccharide (*9*) and *Bacillus* collagen-like protein of *B. anthracis* (BclA) (*8*)] has been reported only for lamprey VLRs. However, the mode of antigen recognition has not yet been determined in either system, nor has it been shown whether complementarity-determining region (CDR) equivalents are present in VLRs that would endow them with specificity and affinity for any given antigen, as for antibodies.

We determined the crystal structure of the VLR RBC36 ectodomain (ECD) in complex with the H-trisaccharide derived from the H-antigen of human blood group O erythrocytes at 1.67 Å resolution by molecular replacement, using our lamprey VLR2913 crystal structure [Protein Data Bank (PDB) ID 2R9U]. Lampreys were previously shown to produce high-titer agglutinins against the H-antigens of human O erythrocytes (*10*, *11*). When lampreys were immunized with human blood group O erythrocytes, they elicited VLRs that recognize the dominant H-trisaccharide antigen on Chinese hamster ovary cells transfected with 1,2-fucosyltransferase (*9*). H-antigens contain the characteristic disaccharide α-L-Fuc*p*-(1→2)-β-D-Gal*p*-OR, where R is glycoprotein or glycolipid (*12*). The type II H-antigen trisaccharide, α-L-Fuc*p*-(1→2)-β-D-Gal*p*-(1→4)-β-D-GlcNac*p*-OH, was

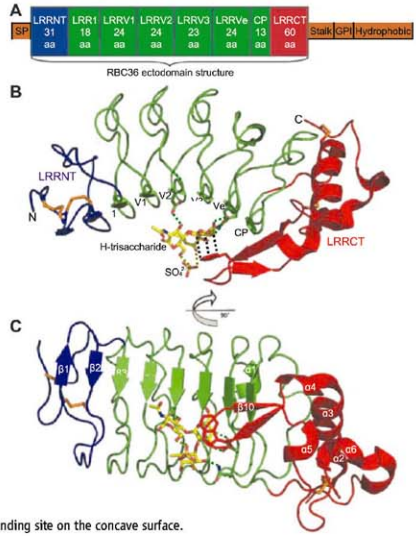

Fig. 1. Overall architecture of the VLR RBC36-ECD in complex with the H-trisaccharide. **(A)** Schematic diagram of RBC36. Regions from left to right: signal peptide (SP), N-terminal LRR (LRRNT), five variable LRRs (LRR1, LRRVs), connecting peptide (CP), C-terminal LRR (LRRCT), threonine/proline-rich stalk region, GPI anchor, and hydrophobic tail. **(B)** Ribbon diagram of RBC36-ECD in complex with H-trisaccharide. LRRNT, LRRs, and LRRCT are colored blue, green, and red, respectively. Carbons, nitrogens, and oxygens of the H-trisaccharide are colored yellow, blue, and red, respectively. Disulfide bridges are shown in orange. Green dotted lines represent hydrogen bonds; black dotted lines indicate hydrophobic effects. **(C)** View rotated 90° from (B) that highlights the continuous β sheet and the H-trisaccharide binding site on the concave surface.

[1]Department of Molecular Biology, Scripps Research Institute, La Jolla, CA 92037, USA. [2]Skaggs Institute for Chemical Biology, Scripps Research Institute, La Jolla, CA 92037, USA. [3]Emory Vaccine Center and Department of Pathology and Laboratory Medicine, Emory University, 1462 Clifton Road NE, Atlanta, GA 30322, USA.
*To whom correspondence should be addressed. E-mail: wilson@scripps.edu

used as the antigen in the crystal structure with the RBC36-ECD (Fig. 1, Fig. 2, A and B, and fig. S1) (*13*).

Lamprey RBC36-ECD (residues 22 to 238, lacking the N-terminal signal sequence) forms a horseshoe-shaped assembly that is more abbreviated and crescent-shaped relative to TLRs. This assembly consists of an LRRNT, an 18-residue LRR1, three LRRVs, an LRRVe, a CP, and an LRRCT, all of which adopt a right-handed solenoidal structure, except for LRRCT. The inner, concave surface is formed from eight β strands (two from LRRNT, five from LRRs, and one from CP), which assemble into a continuous β sheet. The convex (outer) surface is composed of the more diverse secondary structure elements, including loops of varying length, one α helix, and six 3_{10} helices (Fig. 1). Lamprey RBC36-ECD contains five canonical LRR-signature motifs, $xL^{2}xxL^{5}xxL^{8}xL^{10}xxN^{13}Q^{14}L^{15}xxL^{18}P^{19}xG^{21}V^{22}F^{23}D^{24}$ [where L represents obligate hydrophobic residues—which, for RBC36-ECD, include leucine (most prevalent), isoleucine, or methionine—and N, Q, P, G, F, and D are conserved asparagine, glutamine, proline, glycine, phenylalanine, and aspartic acid residues, respectively] (Fig. 2D) (*4*, *14*). The side chains of nine conserved residues in each LRR (at relative positions 2, 5, 8, 10, 13, 15, 18, 22, and 23) assemble within the solenoidal structure and form a tight hydrophobic core that laterally stabilizes the repeating LRR modules (Fig. 2E). In RBC36-ECD, LRRNT comprises residues 22 to 52, in which Thr^{32}, Val^{33}, and Asp^{34} initiate an antiparallel β strand that extends the continuous parallel β sheet, and LRRNT and LRRCT cover the exposed edges of the hydrophobic core of the solenoidal LRR structure, as observed in other LRR proteins, including TLRs (*5*, *6*). In LRRNT, the characteristic four-cysteine motif (Cx_nCxCx_nC) forms two sets of disulfides (Cys^{22} to Cys^{28} and Cys^{26} to Cys^{35}), whereas in LRRCT, a similar motif ($CxCx_nCx_nC$) gives rise to disulfides Cys^{182} to Cys^{217} and Cys^{184} to Cys^{237} (Fig. 1).

After accounting for the protein, extra electron density on the concave surface remained, which corresponded to the H-trisaccharide antigen (fig. S2). Specificity between RBC36 and H-

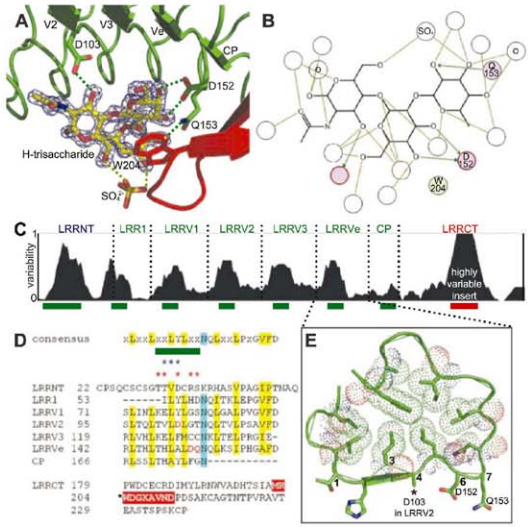

Fig. 2. The H-trisaccharide binding site of RBC36. **(A)** VLR residues involved in recognizing the H-trisaccharide. After refinement, a $2F_{obs} - F_{calc}$ electron density map was calculated and contoured at 2σ as a blue mesh around the H-trisaccharide. Colors are as in Fig. 1. **(B)** H-trisaccharide interaction with RBC36 including solvent molecules, modified from the ligand interaction calculation by the program MOE (*33*). O in a circle represents waters. Hydrogen bonds with RBC36 residues and solvent molecules are drawn with green and pale green lines, respectively. Trp^{204}, which is important for stabilizing the galactose via hydrophobic and stacking effects, is shown in a green circle beside the galactose sugar ring (*14*). **(C)** Sequence variability plot for amino acid residues from LRRNT to LRRCT of known VLRs. Green bars on the bottom represent residues on the concave surface; the red bar in the LRRCT shows the location of the highly variable insert. **(D)** Sequence alignment of LRR modules of RBC36 (*14*). The green bar shows the residues on the concave surface. Blue and red asterisks represent residues forming the β sheet and side chains that face the concave surface, respectively. Letters on yellow, blue, and red backgrounds show conserved hydrophobic residues, asparagine residues, and residues in the highly variable insert, respectively. Key residues on the concave surface (Asp^{103}, Asp^{152}, and Gln^{153}) for the H-trisaccharide interaction are shown as red letters; Trp^{204} in the highly variable insert is indicated by a black asterisk at the left. **(E)** The conformation of the LRRVe module highlights the tight packing of the conserved hydrophobic residues, with their van der Waals radii outlined in dots. The seven residues that form the concave surface are numbered from the N terminus to the C terminus of the LRR.

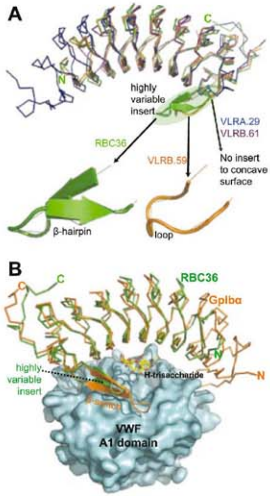

Fig. 3. Highly variable inserts of VLRs. **(A)** Crystal structures of lamprey RBC36 and three hagfish VLRs are superposed. Cα trace for different VLRs: RBC36 in green, VLRA.29 in blue (PDB ID 2O6Q), VLRB.59 in orange (PDB ID 2O6S), and VLRB.61 in magenta (PDB ID 2O6R), respectively. Highly variable inserts are drawn in cartoon representation. **(B)** Superposition of RBC36–H-trisaccharide complex and Gplbα-VWF A1 domain complex (PDB ID 1M10). Overall RBC36-ECD structure is rotated 180° vertically from (A) to highlight the comparison of the highly variable insert of RBC36 and the β switch of Gplbα. RBC36 is depicted as a green trace, Gplbα as an orange trace, VWF A1 domain as a surface representation in cyan, and the H-trisaccharide as in Fig. 1. The β hairpin of the highly variable insert of RBC36 and the β switch of Gplbα are shown in cartoon representation.

trisaccharide is mainly mediated by four hydrogen bonds (Fig. 2A) on the inner concave surface: between Asp^{103} O^{D2} and N-acetylglucosamine O^{AZ}, between Asp^{152} O^{D1} and galactose O^{4}, between Asp^{152} O^{D2} and galactose O^{3}, and between Gln^{153} N^{E2} and fucose O^{AL} (Fig. 2, A and B). Asp^{103} is located on LRRV2, and Asp^{152} and Gln^{153} on LRRVe.

With the concave surface of RBC36 firmly established as the antigen-binding site, we analyzed the variability in amino acids represented on this surface in other VLRs. From BLASTP searches (*15*) with RBC36, 24 VLR sequences were found with three LRRVs and sequence identity of >60%. The amino acid variation was higher on the concave surface of each LRR module (Fig. 2C, fig. S3, and table S2) and hence, to some extent, is analogous to the hypervariable regions (CDRs) in antibodies. In each canonical 24-residue LRR module, seven residues, $xxL^{8}xL^{10}xx$, are located on the concave surface and, of these, only the two obligate hydrophobic residues (L) face inward to form the hydrophobic core of the solenoidal structure (Fig. 2, D and E). Consequently, the other five residues could potentially contribute to antigen recognition, and correspond to the first, second, fourth, sixth, and seventh positions of this seven-residue segment in each LRR. Asp^{103}, Asp^{152}, and Gln^{153}, which contribute significantly to the interaction between RBC36 and H-trisaccharide, represent the fourth residue of the LRRV2 and the sixth and seventh residues of the LRRVe concave surfaces. Eight other residues on the concave surface (His^{57}, Tyr^{79}, Thr^{106}, Phe^{127}, Cys^{129}, Ala^{150}, Tyr^{174}, and Phe^{176}) stabilize the H-trisaccharide interaction via 16 van der Waals contacts, as calculated with CONTACSYM (*16*). The carbohydrate antigen buries ~303 Å^2 on the VLR, whereas the corresponding buried surface on the antigen is ~246 Å^2 calculated with a 1.4 Å probe radius (*17*, *18*), which is comparable to buried surfaces of haptens (~150 to 350 Å^2) with antibodies (*19*).

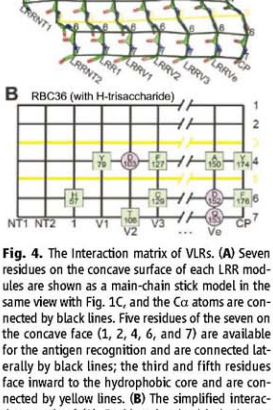

Fig. 4. The interaction matrix of VLRs. **(A)** Seven residues on the concave surface of each LRR modules are shown as a main-chain stick model in the same view with Fig. 1C, and the Cα atoms are connected by black lines. Five residues of the seven on the concave face (1, 2, 4, 6, and 7) are available for the antigen recognition and are connected laterally by black lines; the third and fifth residues face inward to the hydrophobic core and are connected by yellow lines. **(B)** The simplified interaction matrix of (A). Residues involved in hydrogen bonds or in van der Waals contacts are labeled in a circle or in a square, respectively.

Another key interaction with the H-trisaccharide is between Trp^{204} and the galactose. The Trp^{204} indole is stacked parallel to the sugar ring, as observed in other sugar-protein complexes (Fig. 1 and Fig. 2A) (*20*). Trp^{204} is located in the middle of LRRCT, where the VLR sequences are extremely diverse and a highly variable insert is often present (*21*). The variability plot (Fig. 2C) illustrates that highly variable inserts of 2 to 12 residues occur in LRRCT (fig. S3). In RBC36, a 10-residue insert forms a β hairpin and Trp^{204} is located at the end of the first β strand, prior to the β-hairpin turn (Fig. 1 and Fig. 2A). Superposition of the crystal structures of lamprey RBC36 and the three hagfish VLRs reveals not only high sequence variability, but also secondary structure variation in their inserts. The VLRB.59 eight-residue insert is a loop, but similar in overall shape to the RBC36 β hairpin, whereas the VLRA.29 three-residue insert points toward the horseshoe side rather than its concave surface; VLRB.61 has no insert (Fig. 3A).

The RBC36 insert lies in close proximity to the concave β sheet, and its overall conformation is remarkably similar to the β switch in the C-terminal flank region of human glycoprotein Ibα (GpIbα) that interacts with von Willebrand factor (VWF) A1 domain (*22*) (Fig. 3B). A search for structural homologs of RBC36, using the DALI server (*23*), selected GpIbα (PDB ID 1M10) as one of the top three hits along with hagfish VLRB.59 (PDB ID 2O6S) and human Slit protein (PDB ID 2V9T), all of which are LRR-containing proteins. Interestingly, GpIbα and Slit also have crystal structures with their binding partners, in which their mode of interaction is very similar to the RBC36–H-trisaccharide complex where the same first, second, fourth, sixth, and seventh residues on the concave surface in each LRR module play the key role in ligand binding, but the insert in the Slit LRRCT does not contact its ligand (Fig. 3B and fig. S4). Considering that the secondary structures of the highly variable inserts of VLRs in the PDB are diverse (Fig. 3A), and the equivalent β switch of human GpIbα adopts a loop structure when GpIbα is crystallized by itself (*22*), these structure differences may also play an important role in antigen selection, recognition, and affinity. Conformational changes or isomerism in the inserts would also increase possible binding modes in much the same way as induced fit in the CDR loops of antibodies, especially for CDR H3 (*24*), or equivalent loops (α3, β3) in T cell receptors (*25*).

The concave molecular surface area of RBC36 is estimated to be ~1720 Å^2 calculated with a 1.4 Å probe radius (*17*, *18*), compared with a buried surface of ~700 to 1000 Å^2 on average for the antigen-binding regions of immunoglobulins for proteins and other large antigens. Considering that the number of LRRVs in VLRs can be as many as seven and the concave surface area of one LRRV is about 220 Å^2, the total antigen-binding surface could extend to around 2600 Å^2 and could potentially accommodate binding sites for multiple antigens. However, this size could well be an overestimate as were the corresponding early predictions for the antigen-binding surfaces of antibodies (*26*), although the possibility of multiple paratopes in VLRs is certainly an intriguing concept.

With few exceptions, five residues on the concave surface of each LRR module are available for antigen binding (Fig. 2E and Fig. 4A). Hence, we mapped these key residues for antigen recognition onto a coordinate system that corresponds to the LRR modules along the *x* axis and key residue positions on the concave surface along the *y* axis (Fig. 4B). This interaction matrix should also be useful when other VLR-antigen complexes are determined.

Antigen recognition by antibodies in the vertebrate immune system is well documented and has revealed how the immunoglobulin (Ig) fold with its CDR loops can form a high-affinity binding site for virtually any antigen it encounters, whether natural or synthetic (*24*). Similarities and differences can now be assessed for antigen recognition by the Ig fold and the LRRs of VLRs, as well as TLRs. High sequence variability in the Ig fold is concentrated in CDRs H1, H2, H3, L1, L2, and L3, whereas that of VLRs is confined to the concave surface of each LRR module (Fig. 2C). In the Ig fold, a wide range of specificities and affinities for the antibody-combining sites is ensured not only by variability in amino acid composition, but also by insertions in the CDRs, especially in CDR H3 (*27*). However, VLRs contain few insertions on the concave surface of each LRR module, although diversity is attained by variation in the number (up to seven) and amino acid composition of the LRRV modules. The only insertion in VLRs is observed in the middle of LRRCT, which shows highly variable amino acid composition, length, and secondary structure. To what extent the highly variable insert in LRRCT contributes to the specificity, affinity, and shape of the antigen-binding site of VLRs awaits further VLR-antigen complex structures.

Recently, three crystal structures of TLR-ligand complexes—TLR4-MD2–Eritoran (*28*), TLR1-TLR2–lipopeptide (*29*), and TLR3-dsRNA (*30*)—have been determined. So far, only the binding mode of the TLR4-MD2 complex is similar to that of antigen recognition by VLRs, in that residues on the concave surface of the N-terminal and central domains of TLR4 interact with MD2. However, no interaction is seen between LRRCT of TLR4 and MD2 as observed between the highly variable insert in LRRCT of VLRs and

antigens. Because we do not yet have sufficient VLR and TLR complex structures to make statistically significant conclusions, and the number of LRR modules in TLRs is much greater than in VLRs, it may be too early to infer evolutionary relationships between VLRs and TLRs.

The crystal structure of RBC36-ECD in complex with the H-trisaccharide has provided structural insight into how VLRs recognize their antigens and provides a basis for rational design and modification of other antigen-specific VLRs. This VLR-antigen structure sheds light on the adaptation and evolution of primordial LRR proteins into their more specialized roles in pathogen recognition (e.g., TLRs) by the mammalian innate immune system.

References and Notes

1. Z. Pancer *et al.*, *Nature* **430**, 174 (2004).
2. M. N. Alder *et al.*, *Science* **310**, 1970 (2005).
3. When the distribution of LRRV modules per transcript was analyzed from 517 unique VLR sequences, VLRs were found to have an average of 1.31 LRRV modules between the canonical LRR1 and LRRVe modules (*2*): 109 VLRs (0 LRRV), 228 VLRs (1 LRRV), 119 VLRs (2 LRRVs), 45 VLRs (3 LRRVs), 6 VLRs (4 LRRVs), 8 VLRs (5 LRRVs), 1 VLR (6 LRRVs), and 1 VLR (7 LRRVs).
4. Z. Pancer *et al.*, *Proc. Natl. Acad. Sci. U.S.A.* **102**, 9224 (2005).
5. J. Choe, M. S. Kelker, I. A. Wilson, *Science* **309**, 581 (2005); published online 16 June 2005 (10.1126/science.1115253).
6. J. K. Bell *et al.*, *Proc. Natl. Acad. Sci. U.S.A.* **102**, 10976 (2005).
7. H. M. Kim *et al.*, *J. Biol. Chem.* **282**, 6726 (2007).
8. B. R. Herrin *et al.*, *Proc. Natl. Acad. Sci. U.S.A.* **105**, 2040 (2008).
9. M. N. Alder *et al.*, *Nat. Immunol.* **9**, 319 (2008).
10. G. A. Boffa, J. M. Fine, A. Drilhon, P. Amouch, *Nature* **214**, 700 (1967).
11. B. Pollara, G. W. Litman, J. Finstad, J. Howell, R. A. Good, *J. Immunol.* **105**, 738 (1970).
12. At least four subtypes of H-antigens are known, which can be further converted into the A-antigen of human blood group A and B-antigen of human blood group B by glycosyltransferases A and B, respectively (*31*) (fig. S1).
13. See supporting material on *Science* Online.
14. Single-letter abbreviations for amino acid residues: A, Ala; C, Cys; D, Asp; E, Glu; F, Phe; G, Gly; H, His; I, Ile; K, Lys; L, Leu; M, Met; N, Asn; P, Pro; Q, Gln; R, Arg; S, Ser; T, Thr; V, Val; W, Trp; Y, Tyr.
15. S. F. Altschul *et al.*, *Nucleic Acids Res.* **25**, 3389 (1997).
16. S. Sheriff, W. A. Hendrickson, J. L. Smith, *J. Mol. Biol.* **197**, 273 (1987).
17. B. R. Gelin, M. Karplus, *Biochemistry* **18**, 1256 (1979).
18. M. L. Connolly, *J. Mol. Graph.* **11**, 139 (1993).
19. I. A. Wilson, R. L. Stanfield, *Curr. Opin. Struct. Biol.* **3**, 113 (1993).
20. Aromatic residues, such as Trp and Tyr, are frequently observed in the protein sugar-binding sites. For example, in the maltose/maltooligosaccharide-binding protein (*32*), aromatic residues play a major role in carbohydrate recognition and binding by providing not only hydrophobic stacking interactions between aromatic residues and the hydrophobic face of the sugar rings, but also polar contacts to the sugar hydroxyl groups.
21. I. B. Rogozin *et al.*, *Nat. Immunol.* **8**, 647 (2007).
22. E. G. Huizinga *et al.*, *Science* **297**, 1176 (2002).
23. L. Holm, C. Sander, *J. Mol. Biol.* **233**, 123 (1993).
24. I. A. Wilson, R. L. Stanfield, *Curr. Opin. Struct. Biol.* **4**, 857 (1994).
25. K. C. Garcia, L. Teyton, I. A. Wilson, *Annu. Rev. Immunol.* **17**, 369 (1999).
26. P. von Gara, *Z. Immunitaetsforsch. Exp. Ther.* **71**, 1 (1931).
27. T. T. Wu, G. Johnson, E. A. Kabat, *Proteins* **16**, 1 (1993).
28. H. M. Kim *et al.*, *Cell* **130**, 906 (2007).
29. M. S. Jin *et al.*, *Cell* **130**, 1071 (2007).
30. L. Liu *et al.*, *Science* **320**, 379 (2008).
31. F. Yamamoto, P. D. McNeill, S. Hakomori, *Biochem. Biophys. Res. Commun.* **187**, 366 (1992).
32. X. Duan, F. A. Quiocho, *Biochemistry* **41**, 706 (2002).

33. Molecular Operating Environment (MOE), version 2000.09 (Chemical Computing Group, Montreal, 2003).
34. We thank R. L. Stanfield, X. Dai, and X. Zhu for help with data collection and analysis; M. N. Alder for help with VLR cDNA library preparation; J. Paulson and R. McBride for helpful comments and suggestions; and J. Vanhnasy, B. Droese, and H.-J. Kim for technical support and advice. Portions of this research were carried out at the Stanford Synchrotron Radiation Laboratory (SSRL), operated by Stanford University on behalf of the U.S. Department of Energy, Office of Basic Energy Sciences. Supported by NIH grants AI42266 (I.A.W.) and AI072435 (M.D.C.), the Georgia Research Alliance (M.D.C.), and the Skaggs Institute for Chemical Biology (I.A.W.). This is Scripps Research Institute manuscript 19581-MB. Coordinates and structure factors have been deposited in the Protein Data Bank (PDB) with accession code 3E6J.

Supporting Online Material

www.sciencemag.org/cgi/content/full/321/5897/1834/DC1
Materials and Methods
Figs. S1 to S4
Tables S1 to S2
References

30 June 2008; accepted 28 August 2008
10.1126/science.1162484

Disruption of the *CFTR* Gene Produces a Model of Cystic Fibrosis in Newborn Pigs

Christopher S. Rogers,[1]* David A. Stoltz,[1]* David K. Meyerholz,[2]* Lynda S. Ostedgaard,[1] Tatiana Rokhlina,[1] Peter J. Taft,[1] Mark P. Rogan,[1] Alejandro A. Pezzulo,[1] Philip H. Karp,[1,3] Omar A. Itani,[1] Amanda C. Kabel,[1] Christine L. Wohlford-Lenane,[4] Greg J. Davis,[1] Robert A. Hanfland,[5] Tony L. Smith,[5] Melissa Samuel,[6] David Wax,[6] Clifton N. Murphy,[6] August Rieke,[6] Kristin Whitworth,[6] Aliye Uc,[4] Timothy D. Starner,[4] Kim A. Brogden,[7] Joel Shilyansky,[5] Paul B. McCray Jr.,[4] Joseph Zabner,[1] Randall S. Prather,[6] Michael J. Welsh[1,3,8]†

Almost two decades after *CFTR* was identified as the gene responsible for cystic fibrosis (CF), we still lack answers to many questions about the pathogenesis of the disease, and it remains incurable. Mice with a disrupted *CFTR* gene have greatly facilitated CF studies, but the mutant mice do not develop the characteristic manifestations of human CF, including abnormalities of the pancreas, lung, intestine, liver, and other organs. Because pigs share many anatomical and physiological features with humans, we generated pigs with a targeted disruption of both *CFTR* alleles. Newborn pigs lacking CFTR exhibited defective chloride transport and developed meconium ileus, exocrine pancreatic destruction, and focal biliary cirrhosis, replicating abnormalities seen in newborn humans with CF. The pig model may provide opportunities to address persistent questions about CF pathogenesis and accelerate discovery of strategies for prevention and treatment.

Understanding human disease often requires the use of animal models. Mice have been the overwhelming species of choice because methods for specifically altering their genome have been readily available. However, in many cases, mice with targeted gene manipulations fail to replicate phenotypes observed in humans—one example is cystic fibrosis (CF).

In 1938, Dorothy Andersen coined the term "cystic fibrosis of the pancreas" (*1*). Over the ensuing years, investigators learned that CF involved many other organs, including the intestine, lung, sweat gland, liver, gallbladder, and male genital tract (*2*–*4*). We now know CF to be a common, autosomal recessive disease with a carrier rate of ~5% in Caucasians. In 1989, the gene mutated in CF was identified, and its product was named cystic fibrosis transmembrane conductance regulator (CFTR) (*5*). Soon thereafter, it was discovered that CFTR is a regulated anion channel that may also affect other transport processes (*3*).

Despite many advances, our understanding of CF pathogenesis remains incomplete, thus hindering the development of new therapies. This begs the question: Why have we not made more progress? Whereas superb clinical research has guided thoughts about CF, interpretations about pathogenesis are often based on observations ob-

[1]Department of Internal Medicine, Roy J. and Lucille A. Carver College of Medicine, University of Iowa, Iowa City, IA 52242, USA. [2]Department of Pathology, Roy J. and Lucille A. Carver College of Medicine, University of Iowa, Iowa City, IA 52242, USA. [3]Howard Hughes Medical Institute (HHMI), Roy J. and Lucille A. Carver College of Medicine, University of Iowa, Iowa City, IA 52242, USA. [4]Department of Pediatrics, Roy J. and Lucille A. Carver College of Medicine, University of Iowa, Iowa City, IA 52242, USA. [5]Department of Surgery, Roy J. and Lucille A. Carver College of Medicine, University of Iowa, Iowa City, IA 52242, USA. [6]Division of Animal Sciences, University of Missouri, Columbia, MO 65211, USA. [7]Department of Periodontics and Dows Institute for Dental Research, College of Dentistry, University of Iowa, Iowa City, IA 52242, USA. [8]Department of Molecular Physiology and Biophysics, Roy J. and Lucille A. Carver College of Medicine, University of Iowa, Iowa City, IA 52242, USA.

*These authors contributed equally to this work.
†To whom correspondence should be addressed. E-mail: michael-welsh@uiowa.edu

tained long after the disease onset, and many studies cannot be carried out in humans. Cell-based models have also proven valuable for research (*6*) but are limited because the disease involves a whole organism. Gene-targeted mouse models have likewise been instructive about CF, yet the mutant mice do not develop the pancreatic, airway, intestinal, or liver disease typically found in humans (*7*–*9*).

To develop a new CF model, we chose pigs because in terms of anatomy, biochemistry, physiology, size, life span, and genetics, they are more similar to humans than are mice (*10*, *11*). We used homologous recombination in fibroblasts of outbred domestic pigs to disrupt the *CFTR* gene and somatic cell nuclear transfer to generate $CFTR^{-/-}$ pigs (*12*).

At sexual maturity (~6 to 7 months), female $CFTR^{+/-}$ pigs were bred to $CFTR^{+/-}$ males. Six litters produced 64 piglets. Genotyping (Fig. 1A) revealed 18 $CFTR^{+/+}$, 26 $CFTR^{+/-}$, and 20 $CFTR^{-/-}$ animals, a ratio not significantly different from the expected ratio of 1:2:1 (*13*). Figure 1B shows the first litter. Birth weights varied but did not segregate by genotype (Fig. 1C). The piglets looked normal at birth, and their genotype could not be discerned by appearance. A normal appearance is consistent with findings in humans.

Northern blot analysis and quantitative reverse transcription polymerase chain reaction (RT-PCR) did not detect normal *CFTR* transcripts (Fig. 1A). Immunoprecipitation detected no normal CFTR protein. Like human CFTR (*14*, *15*), in wild-type (WT) tissue the porcine protein localized apically in airway epithelia and ileal crypts (Fig. 1D).

We assessed CFTR function in vivo by measuring transepithelial voltage (Vt) across nasal epithelia (*16*) (Fig. 1, E and F). As in humans with CF, baseline Vt was hyperpolarized in $CFTR^{-/-}$ piglets. Amiloride, which inhibits ENaC Na^+ channels, reduced Vt in all genotypes. To test for CFTR channel activity, we perfused the apical surface with a Cl^--free solution and added isoproterenol to increase cellular levels of cyclic adenosine monophosphate; these interventions hyperpolarized nasal Vt in WT and heterozygous pigs, but not $CFTR^{-/-}$ animals. Perfusion with adenosine triphosphate to activate P2Y2 receptors and Ca^{2+}-activated Cl^- channels (*17*) further hyperpolarized Vt, and the response did not differ significantly

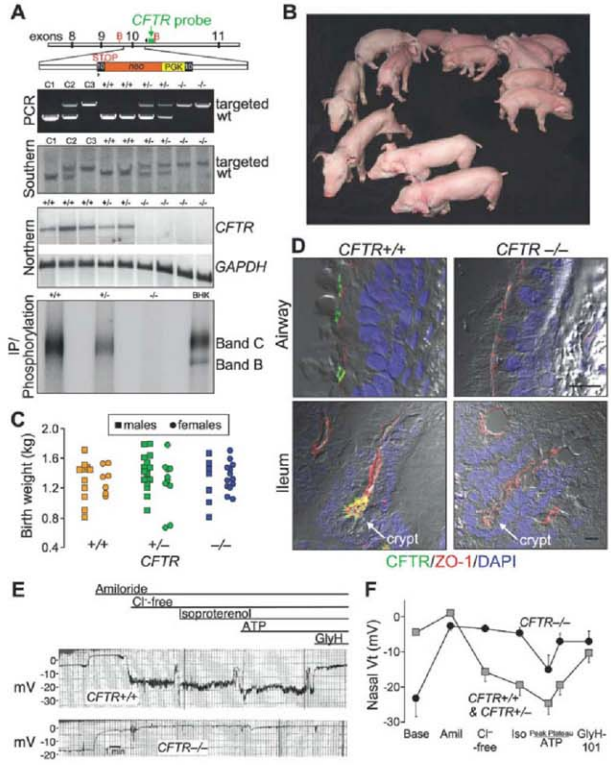

Fig. 1. $CFTR^{-/-}$ piglets appear normal at birth. **(A)** Upper panel depicts insertion into porcine *CFTR* exon 10 of a phosphoglycerate kinase (PGK) promoter (yellow) driving a neomycin resistance cDNA (orange), and an engineered stop codon. Position of probe (green), PCR primers (arrowheads), and *Bgl*II sites (B) is indicated. The second and third panels show genotyping by PCR and Southern blot analysis of genomic DNA. Lanes C1, C2, and C3 contain controls of $CFTR^{+/+}$, $^{+/-}$, and $^{-/-}$ DNA, respectively. The fourth panel shows Northern blot analysis of ileal *CFTR* and *GAPDH* mRNA. Consistent with the Northern blot, quantitative RT-PCR of exon 10 (the targeted site) detected <0.1% of *CFTR* transcripts in $CFTR^{-/-}$ ileum, relative to $CFTR^{+/+}$ (n = 6 and 4 piglets, respectively). The bottom panel shows immunoprecipitation (IP) and phosphorylation of CFTR plus recombinant CFTR in baby hamster kidney cells. **(B)** First litter containing piglets of all three genotypes. **(C)** Birth weights. Mean ± SD of weights: 1.31 ± 0.24 kg for $CFTR^{+/+}$ (orange), 1.35 ± 0.28 kg for $CFTR^{+/-}$ (green), and 1.31 ± 0.23 kg for $CFTR^{-/-}$ (blue) animals. **(D)** Immunocytochemistry of CFTR in airway epithelia (top) and ileum (bottom). Figures are differential interference contrast with staining for ZO-1 (a component of tight junctions, red), CFTR (green), and nuclei (4′,6′-diamidino-2-phenylindole, blue). See also fig. S1. Scale bars, 10 μm. **(E)** Tracings of in vivo nasal Vt measured in newborn pigs. After baseline measurements, the following agents/solutions were sequentially added to the epithelial perfusate: amiloride (100 μM), Cl^--free solution, isoproterenol (10 μM), ATP (100 μM), and GlyH-101 (100 μM). **(F)** Average nasal Vt measurements as indicated in (E). Data from four $CFTR^{+/+}$ and four $CFTR^{+/-}$ piglets (gray squares) were not statistically different and were combined and compared with data from five $CFTR^{-/-}$ piglets (blue circles). Values of baseline nasal Vt for $CFTR^{-/-}$ piglets differed from the controls, as did the changes in Vt induced by adding amiloride, a Cl^--free solution, and GlyH-101 (all $P < 0.05$). Data are mean ± SEM.

between genotypes. Perfusion with the CFTR inhibitor GlyH-101 (*18*) depolarized Vt in controls animals, but not in *CFTR*$^{-/-}$ piglets. These data reveal the loss of CFTR Cl channel activity in newborn *CFTR*$^{-/-}$ pigs. Whereas the lack of data from newborn humans precludes a direct comparison, our data qualitatively match those from adults and children with CF (*16*).

What phenotypes would be expected if newborn *CFTR*$^{-/-}$ piglets model human disease? Figure 2A shows some human CF phenotypes and the time spans when they become clinically apparent (*3*, *19*). The earliest manifestation (hours to 2 days) is meconium ileus, an intestinal obstruction occurring in ~15% of CF infants (*2*, *3*, *19*, *20*). Obstruction can occur throughout the small intestine or colon, but it is most often observed near the ileocecal junction. Distal to the obstruction, the bowel is small and atretic (microcolon). Intestinal perforation in utero or postnatally occurs in some infants.

Newborn *CFTR*$^{-/-}$ piglets failed to pass feces or gain weight (Fig. 2B). By 24 to 40 hours of age, they stopped eating, developed abdominal distension, and had bile-stained emesis, which are clinical signs of intestinal obstruction. We examined histopathology between birth and 12 hours in piglets that had not eaten and between 24 and 40 hours in piglets that were fed colostrum and milk replacer. Except as noted, the pathologic changes refer to the earlier time period. After 30 to 40 hours, the stomachs of *CFTR*$^{-/-}$ piglets contained small amounts of green, bile-stained milk (Fig. 2C). The proximal small intestine was dilated by small amounts of milk and abundant gas. The site of obstruction ranged from mid-distal small intestine to proximal spiral colon, the anatomical equivalent of the human ascending colon. Perforation and peritonitis occurred in some piglets. Dark green meconium distended the *CFTR*$^{-/-}$ intestine, and adjacent villi showed degeneration and atrophy, whereas *CFTR*$^{+/+}$ ileum had long villi (Fig. 2D). Distal to the meconium, luminal diameter was reduced with mild-to-severe mucinous hyperplasia, including mucoid luminal "plugs" (Fig. 2E). These changes replicate those seen in humans with CF (*3*, *19*).

The penetrance of meconium ileus was 100% in *CFTR*$^{-/-}$ piglets versus ~15% in human CF. Potential explanations for this difference include a restricted genetic background in our pig model versus that in humans, a null mutation in the pigs versus mutations in humans that might yield tiny amounts of protein function, and anatomical or physiological differences [see footnote F1 in (*13*)].

Exocrine pancreatic insufficiency afflicts 90 to 95% of patients with CF (*1*–*4*, *19*, *21*, *22*). The porcine *CFTR*$^{-/-}$ pancreas was small (Fig. 3A), and microscopic examination revealed small, degenerative lobules with increased loose adipose and myxomatous tissue, as well as scattered-to-moderate cellular inflammation (Fig. 3, B and C). Residual acini had diminished amounts of eosinophilic zymogen granules (Fig. 3D). Centroacinar spaces, ductules, and ducts were variably dilated and obstructed by eosinophilic material plus infrequent neutrophils and macrophages mixed with cellular debris (Fig. 3E). Ducts and ductules had foci of mucinous metaplasia. Pancreatic endocrine tissue was spared (Fig. 3C). These changes are similar to those originally described by Andersen and others (*1*, *19*, *21*) in their studies of human CF.

Humans often require surgery to relieve meconium ileus (*3*). We performed an ileostomy on one *CFTR*$^{+/+}$ piglet and three *CFTR*$^{-/-}$ piglets. Because of technical problems in postoperative care, only one piglet (genotype *CFTR*$^{-/-}$) out of the four recovered. Once newborn infants recover from meconium ileus, the course of their disease resembles that in other patients. Likewise, the piglet grew and went on to develop pancreatic insufficiency. At 10 weeks, the piglet had an episode resembling "distal intestinal obstruction syndrome," which was successfully treated as in humans (*3*) [also see footnote F2 in (*13*)]. Although these observations were based on a single animal, they bore a marked resemblance to clinical observations of human CF.

Focal biliary cirrhosis is the second most common cause of CF mortality (*3*, *20*, *23*). The porcine *CFTR*$^{-/-}$ liver revealed infrequent, mild-to-moderate hepatic lesions (Fig. 3F). Chronic cellular inflammation, ductular hyperplasia, and mild fibrosis were typical of focal biliary cirrhosis. Gallbladder abnormalities, including gallstones, occur in 15 to 30% of patients, and a small gallbladder is a common autopsy finding (*3*). Similarly, porcine *CFTR*$^{-/-}$ gallbladders were small and often filled with congealed bile and mucus (Fig. 3, G and H). Epithelia showed diffuse mucinous changes with folds extending into the lumen.

Approximately 97% of males with CF are infertile (*3*); the vas deferens is often normal at birth, and obstruction is thought to cause progressive deterioration [see footnote F3 in (*13*)]. In all piglets, the vas deferens appeared to be intact. Paranasal sinus abnormalities occur in most chil-

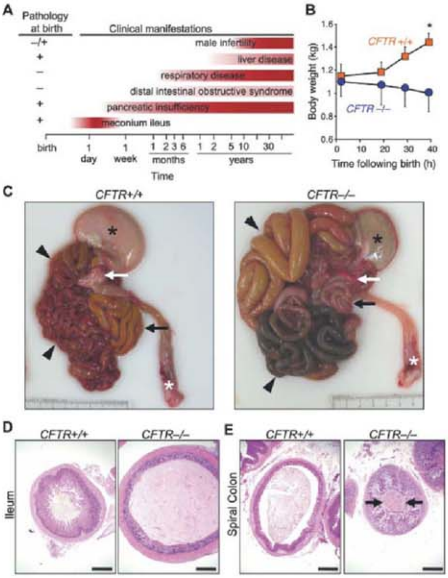

Fig. 2. *CFTR*$^{-/-}$ piglets develop meconium ileus. **(A)** Schematic shows some clinical and histopathological CF manifestations. Pathological abnormalities are present before clinical disease becomes apparent. **(B)** Weight after birth. Animals were fed colostrum and milk-replacer. $n = 7$ *CFTR*$^{+/+}$ and 4 *CFTR*$^{-/-}$ piglets. Data are mean ± SEM. *$P < 0.05$. **(C)** Gross appearance of gastrointestinal tract. Piglets were fed colostrum and milk-replacer for 30 to 40 hours and then euthanized. Stomach, black asterisk; small intestine, arrowheads; pancreas, white arrow; rectum, white asterisk; and spiral colon, black arrow. Of 16 *CFTR*$^{-/-}$ piglets, the obstruction occurred in the small intestine in 7 animals and in spiral colon in 9. **(D** and **E)** Microscopic appearance of the ileum (D) and colon (E). Hematoxylin and eosin (H&E) stain. Scale bars, 1 mm. Images are representative of severe meconium ileus occurring in 16 out of 16 (16/16) *CFTR*$^{-/-}$ piglets.

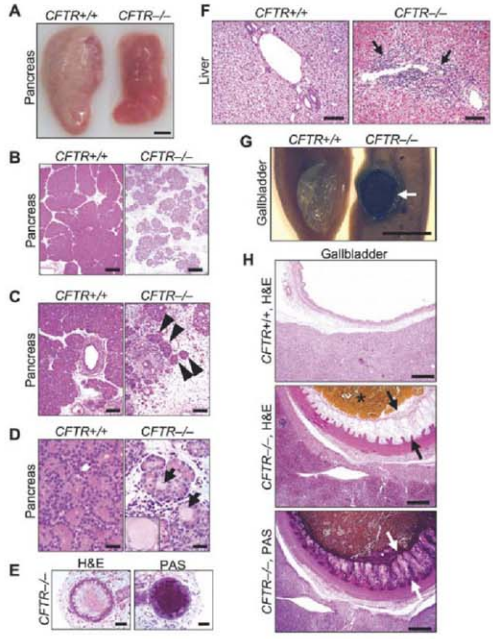

Fig. 3. *CFTR*$^{-/-}$ piglets have exocrine pancreatic destruction and liver and gallbladder abnormalities. **(A)** Gross appearance of pancreas. Scale bar, 0.5 cm. **(B)** Loss of parenchyma in the *CFTR*$^{-/-}$ pancreas. H&E stain. Scale bars, 500 μm. **(C)** Pancreatic ducts and islets of Langerhans (arrowheads). Scale bars, 100 μm. **(D)** *CFTR*$^{-/-}$ ductules and acini dilated by eosinophilic inspissated material that formed concentrically lamellar concretions (arrows and inset). H&E stain. Scale bars, 33 μm. **(E)** Ducts within the *CFTR*$^{-/-}$ pancreas. H&E stain, left; periodic acid–Schiff (PAS) stain, right. Scale bars, 50 μm. **(F)** Microscopic appearance of liver. H&E stain. Arrows indicate focal expansion of portal areas by chronic cellular inflammation. Scale bars, 100 μm. **(G)** Gross appearance of gallbladder. When the *CFTR*$^{+/+}$ gallbladder was sectioned, bile drained away rapidly with collapse of the mucosal wall. *CFTR*$^{-/-}$ bile was congealed (arrow) and retained in the lumen of a smaller gallbladder. Scale bar, 0.5 cm. **(H)** Microscopic appearance of gallbladder. *CFTR*$^{-/-}$ gallbladders had congealed, inspissated bile (asterisk) with variable mucus production (arrows, H&E stain) highlighted as a magenta color in PAS stained tissue. Scale bars, 500 μm. Images are representative of severe pancreatic lesions (15/15 *CFTR*$^{-/-}$ piglets), mild-to-moderate liver lesions (3/15), and mild-to-severe gallbladder/duct lesions (15/15).

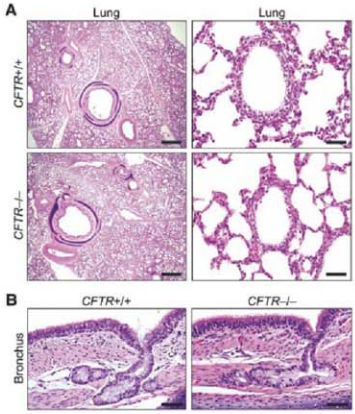

Fig. 4. The lungs of newborn *CFTR*$^{-/-}$ and *CFTR*$^{+/+}$ piglets appear normal. **(A)** Microscopic appearance of lung from piglets <12 hours old. H&E staining. Scale bars, 1 mm (left) and 50 μm (right). **(B)** Bronchial epithelia and submucosal glands. H&E staining. Scale bars, 50 μm. Images are representative of the lack of lesions in 15 out of 15 *CFTR*$^{-/-}$.

dren and adults with CF (*3*). Although *CFTR*$^{-/-}$ porcine paranasal sinuses showed no abnormalities, this negative result is difficult to interpret because it is unclear when sinus disease develops in humans. The salivary glands, nasal cavity, esophageal glands, kidney, heart, striated muscle, spleen, adrenals, eyes, brain, skin, and eccrine sweat glands on the snout revealed no abnormalities in *CFTR*$^{-/-}$ piglets. In all tissues, we observed no differences between WT and heterozygous *CFTR*$^{+/-}$ animals.

Lung disease is the major cause of CF morbidity and mortality (*2*–*4*). The onset of clinical respiratory manifestations varies, with some patients developing symptoms a few months after birth and others after several years. Eventually, most patients develop chronic airway infection and inflammation that destroy the lung. The lungs of neonatal *CFTR*$^{-/-}$ piglets appeared similar to those of their WT littermates. *CFTR*$^{-/-}$ lungs lacked evidence of cellular inflammation in airways or parenchyma (Fig. 4A). Airway epithelia and submucosal glands appeared similar in all three genotypes, and we found no evidence of dilated or plugged submucosal gland ducts [see footnote F4 in (*13*)] (Fig. 4B). Bronchoalveolar lavage 6 to

12 hours after birth showed no evidence of infection, and there were no significant differences between cell counts or levels of interleukin-8 (IL-8) across genotypes (figs. S2 and S3) (*13*).

Whether airway inflammation precedes infection in CF patients or vice versa has been a persistent question. Studies of bronchoalveolar lavage in infants and young children have both supported and argued against the presence of inflammation (increased IL-8 and neutrophilia) without infection (*24*, *25*). In vitro airway epithelial models have also given conflicting results (*26*, *27*). Studies of human fetal trachea transplanted into mice suggested inflammation might occur in developing CF airways (*28*). Although our data do not resolve this controversy, we had the advantage of studying lungs between birth and 12 hours of age, and we found no evidence of abnormal infection or inflammation. Tracking the lungs as *CFTR*$^{-/-}$ piglets are exposed to additional environmental challenges may inform our understanding of how respiratory disease develops in children and young adults.

The clinical, electrophysiological, and pathological findings in newborn *CFTR*$^{-/-}$ pigs were markedly similar to those in human neonates with CF (table S1) (*13*). Abdominal lesions dominate the initial presentation in both, with identical appearance of meconium ileus and exocrine pancreatic destruction. In addition, as in humans, the piglets have hepatic changes consistent with early focal biliary cirrhosis and abnormalities of the gallbladder and bile ducts. The lack of abnormalities in the vas deferens and lungs at birth is another similarity. Overall, these encouraging results suggest that the pig model may provide investigators with further opportunities to study CF and develop strategies for prevention and treatment.

References and Notes

1. D. H. Andersen, *Am. J. Dis. Child.* **56**, 344 (1938).
2. P. M. Quinton, *Physiol. Rev.* **79**, S3 (1999).
3. M. J. Welsh, B. W. Ramsey, F. Accurso, G. R. Cutting, in *The Metabolic and Molecular Basis of Inherited Disease*, C. R. Scriver *et al.*, Eds. (McGraw-Hill, New York, 2001), pp. 5121–5189.
4. S. M. Rowe, S. Miller, E. J. Sorscher, *N. Engl. J. Med.* **352**, 1992 (2005).
5. J. R. Riordan *et al.*, *Science* **245**, 1066 (1989).
6. P. H. Karp *et al.*, in vol. 188 of *Epithelial Cell Culture Protocols*, C. Wise, Ed. (Humana, Totowa, NJ, 2002), pp. 115–137.
7. B. R. Grubb, R. C. Boucher, *Physiol. Rev.* **79**, S193 (1999).
8. C. Guilbault, Z. Saeed, G. P. Downey, D. Radzioch, *Am. J. Respir. Cell Mol. Biol.* **36**, 1 (2007).
9. L. L. Clarke, L. R. Gawenis, C. L. Franklin, M. C. Harline, *Lab. Anim. Sci.* **46**, 612 (1996).
10. Z. Ibrahim *et al.*, *Xenotransplantation* **13**, 488 (2006).
11. C. S. Rogers *et al.*, *Am. J. Physiol. Lung Cell Mol. Physiol.* **295**, L240 (2008).
12. C. S. Rogers *et al.*, *J. Clin. Invest.* **118**, 1571 (2008).
13. Supporting material is available on *Science* Online.
14. I. Crawford *et al.*, *Proc. Natl. Acad. Sci. U.S.A.* **88**, 9262 (1991).
15. G. M. Denning, L. S. Ostedgaard, S. H. Cheng, A. E. Smith, M. J. Welsh, *J. Clin. Invest.* **89**, 339 (1992).
16. T. A. Standaert *et al.*, *Pediatr. Pulmonol.* **37**, 385 (2004).
17. S. J. Mason, A. M. Paradiso, R. C. Boucher, *Br. J. Pharmacol.* **103**, 1649 (1991).
18. C. Muanprasat *et al.*, *J. Gen. Physiol.* **124**, 125 (2004).
19. E. H. Oppenheimer, J. R. Esterly, *Perspect. Pediatr. Pathol.* **2**, 241 (1975).
20. M. Wilschanski, P. R. Durie, *J. R. Soc. Med.* **91**, 40 (1998).
21. J. R. Imrie, D. G. Fagan, J. M. Sturgess, *Am. J. Pathol.* **95**, 697 (1979).
22. S. M. Blackman *et al.*, *Gastroenterology* **131**, 1030 (2006).
23. E. H. Oppenheimer, J. R. Esterly, *J. Pediatr.* **86**, 683 (1975).
24. T. Z. Khan *et al.*, *Am. J. Respir. Crit. Care Med.* **151**, 1075 (1995).
25. D. S. Armstrong *et al.*, *Pediatr. Pulmonol.* **40**, 500 (2005).
26. A. A. Stecenko *et al.*, *Inflammation* **25**, 145 (2001).
27. N. Abdallat *et al.*, *Am. J. Respir. Crit. Care Med.* **166**, 1248 (2002).
28. R. Tirouvanziam *et al.*, *Am. J. Respir. Cell Mol. Biol.* **23**, 121 (2000).

29. We thank A. Arias, E. Bagnall, J. Bartlett, B. Bauer, T. Bohnert, E. Burnight, K. Dobbs, C. Dohrn, L. Dowell, L. Galkhar, D. Guilliams, Y. Hao, S. C. Isom, S. Jones, S. Korte, B. Kussman, J. Launspach, M. Linville, E. Mahan, T. Mayhew, C. McHughes, K. Munson, M. Parker, C. Randak, S. Ramachandran, J. Ross, A. Small, L. Spate, D. Vermeer, E. Walters, and J. Whyte for excellent assistance. We thank our patients with CF for inspiration, and we also thank Cystic Fibrosis Foundation Therapeutics and R. Bridges for the gift of GlyH-101. This work was supported by the National Heart Lung and Blood Institute (grant HL51670), the National Institute of Diabetes and Digestive and Kidney Diseases (grant DK54759), Food for the 21st Century, the Cystic Fibrosis Foundation, and HHMI. C.S.R. was supported by NIH training grant HL07638. D.A.S. is a Parker B. Francis Fellow and was supported by the National Institute of Allergy and Infectious Diseases (grant AI076671). M.J.W. is an Investigator of the HHMI. C.S.R., R.S.P., M.J.W., and the University of Iowa Foundation have applied for a patent related to the work reported in this paper, and C.S.R. and M.J.W. are founders of Exemplar Genetics, a company that is licensing materials and technology related to this work. C.S.R. is currently Director of Research and Development at Exemplar Genetics.

Supporting Online Material

www.sciencemag.org/cgi/content/full/321/5897/1837/DC1
Materials and Methods
SOM Text
Figs. S1 to S3
Table S1
References

11 June 2008; accepted 22 August 2008
10.1126/science.1163600

Seeding and Propagation of Untransformed Mouse Mammary Cells in the Lung

Katrina Podsypanina,* Yi-Chieh Nancy Du, Martin Jechlinger, Levi J. Beverly, Dolores Hambardzumyan, Harold Varmus

The acquisition of metastatic ability by tumor cells is considered a late event in the evolution of malignant tumors. We report that untransformed mouse mammary cells that have been engineered to express the inducible oncogenic transgenes MYC and Kras^{D12}, or polyoma middle T, and introduced into the systemic circulation of a mouse can bypass transformation at the primary site and develop into metastatic pulmonary lesions upon immediate or delayed oncogene induction. Therefore, previously untransformed mammary cells may establish residence in the lung once they have entered the bloodstream and may assume malignant growth upon oncogene activation. Mammary cells lacking oncogenic transgenes displayed a similar capacity for long-term residence in the lungs but did not form ectopic tumors.

Metastatic dissemination of cancer cells, the major cause of cancer mortality, is traditionally viewed as a late-stage event (*1*), although mammary epithelial cells have been shown to disseminate systemically from early neoplastic lesions in transgenic mice and from ductal carcinoma in situ in women (*2*). There is ample evidence that the ability of fully transformed tumor cells to metastasize depends on the regulation of developmental programs and external environmental cues (*3*–*11*), but to what extent the seeding or growth of tumor cells at the ectopic site is dependent on the initiating transforming event(s) is a subject of debate (*12*). We have developed a system that separates the process of seeding cells in the lung from the process of malignant growth at an ectopic site by using animals engineered to express potent oncogenes in a doxycycline-dependent mammary-specific manner. After intravenous (IV) injection of marked mammary cells that have different genetic potentials [no oncogenes, or oncogenes that will be expressed only after cells have taken up residence in an ectopic site (the lungs)], normal mammary cells can lodge in the lungs, grow slowly, and become frank metastatic malignancies once potent oncogenes are turned on.

We recently described tri-transgenic *TetO-MYC;TetO-Kras^{D12};MMTV-rtTA* (*TOM;TOR;MTB*) mice that coordinately express *MYC* and mutant *Kras* oncogenes in mammary epithelial cells when fed doxycycline (*13*). Doxycycline-naïve animals do not express the transgenic oncogenes and have morphologically and functionally normal mammary glands, but they develop diffuse autochthonous tumors within 3 to 4 weeks after doxycycline exposure. Tumors that form because of the expression of these oncogenes display malignant characteristics, such as transplantability and metastasis (fig. S1). Therefore, this model provides primary mammary cells that can be switched from a normal to a neoplastic state with simple experimental manipulation.

Program in Cancer Biology and Genetics, Memorial Sloan-Kettering Cancer Center, New York, NY 10021, USA.

*To whom correspondence should be addressed. E-mail: podsypak@mskcc.org

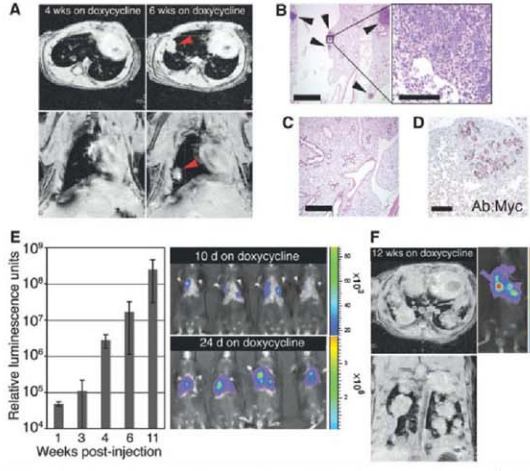

Fig. 1. Untransformed mouse mammary cells form lung metastases after IV injection and induction of oncogenes. (A to D) Lung metastases develop from intravenously injected phenotypically normal mammary cells upon activation of *MYC* and *Kras*^{G12} transgenes. **(A)** Metastases were monitored by MRI in *Rag1*$^{-/-}$ mice after IV delivery of 1×10^6 dissociated primary mammary cells from doxycycline-naïve *TOM;TOR;MTB* mice. Recipient mice were fed doxycycline for 6 weeks starting 1 day before injection. Representative axial (top) and coronal (bottom) images obtained from the same animal 4 and 6 weeks after injection show development of a solid nodule (arrowheads) in the lung. **(B)** Foci of hematoxylin-eosin (H/E)–stained mammary adenocarcinoma (arrowheads) in paraffin-embedded lung sections of the same *Rag1*$^{-/-}$ mouse as in (A). Scale bars indicate 1 mm (left) and 0.1 mm (right). **(C)** No tumors were observed in lung sections of *Rag1*$^{-/-}$ mice that did not receive doxycycline after IV delivery of 1×10^6 primary mammary cells from doxycycline-naïve *TOM;TOR;MTB* mice. Scale bar, 1 mm. **(D)** Tumor cells from the same animal as in (A), but not the surrounding lung tissue, stained with anti-MYC antisera. Scale bar, 0.1 mm. (E and F) Lung metastases develop from intravenously injected phenotypically normal mammary cells upon activation of a *PyMT* transgene. **(E)** Donor cells expressing their transgene were detected by bioluminescence imaging after 5×10^5 primary mammary cells from doxycycline-naïve *TOMT:IRES:Luc;MTB* mice were injected intravenously into *Rag1*$^{-/-}$ mice that were placed on doxycycline 1 day before injection. Representative images at day 10 and day 24 after injection show the presence of signal-emitting cells in the thorax (right); temporal increases in bioluminescence (*14*) were quantified in relative luminescence units (left; $n = 5$ mice; error bars represent SD). **(F)** Axial (top) and coronal (bottom) MRI images of a mouse from (E) maintained on doxycycline for 12 weeks show solid nodules in the lung. A corresponding bioluminescence image is shown on the right.

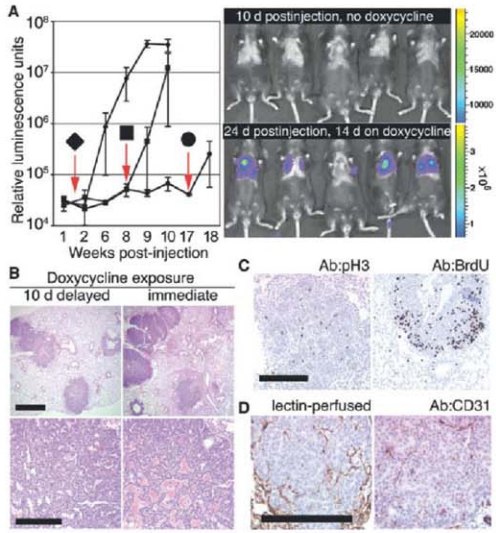

Fig. 2. Delay in oncogene activation does not preclude the development of ectopic mammary tumors. **(A)** Bioluminescence in *Rag1*$^{-/-}$ mice after IV delivery of 1×10^5 mammary cells from doxycycline-naïve *TOMT:IRES:Luc;MTB* mice is undetectable before doxycycline exposure but can be induced at various times after placing mice on doxycycline 1.5 (◆, $n = 7$ mice), 8 (■, $n = 3$ mice), or 17 weeks (●, $n = 2$ mice) after IV injection. Downward arrows indicate times of addition of doxycycline to the diet. Error bars represent SD. Representative bioluminescence images (right) obtained 10 days after injection in the absence of doxycycline (top right) and after 2 additional weeks on doxycycline (bottom right). **(B)** Histologically similar metastatic tumors in lungs of *Rag1*$^{-/-}$ mice after IV delivery of 1×10^5 mammary cells from doxycycline-naïve *TOMT:IRES:Luc;MTB* mice exposed to doxycycline for 8 weeks starting 10 days after (left) or 1 day before (right) IV injection. Scale bars, 1 mm (top) and 0.1 mm (bottom). **(C)** Mitotic activity in tumor foci in lung sections from *Rag1*$^{-/-}$ recipient of *TOM;TOR;MTB* cells (left; stained with anti-pH3) or from *Rag1*$^{-/-}$ recipient of *TOMT:IRES:Luc;MTB* cells (right; stained with anti-BrdU serum after BrdU labeling) (*14*). Scale bar, 0.1 mm. **(D)** Angiogenic proficiency demonstrated by perfusion of the ectopic tumor with biotinylated lectin (left) (*14*) and by staining endothelial cells within tumor foci with anti-CD31 serum in a *Rag*$^{-/-}$ recipient of the *TOMT:IRES:Luc;MTB* cells (right). Scale bar, 0.1 mm.

To investigate whether mammary cells from these mice can be induced to form metastasis in the absence of transformation at the primary site, we modified the traditional experimental metastasis assay (*14*). In the modified approach, instead of IV delivery of tumor cells from doxycycline-treated animals into new recipients, we injected dissociated morphologically normal mammary cells from mature *TOM;TOR;MTB* animals never exposed to doxycycline into the tail veins of *Rag1*$^{-/-}$ (*15*) females on a doxycycline diet. In this way, the injected cells can become transformed only in the bloodstream or tissues of the recipient mouse, an experimental situation that has not been previously examined. Magnetic resonance imaging (MRI) was used to survey *Rag1*$^{-/-}$ recipients for evidence of tumor foci in the lungs. Solitary nodules were observed in four out of four recipients 6 weeks after injection (Fig. 1A), and histological sections showed foci of mammary adenocarcinoma in the lung (Fig. 1B); in contrast, no tumors were found in control mice that did not receive doxycycline (Fig. 1C and table S1). The experimental metastases were histologically identical to the spontaneous metastases observed in tumor-bearing *TOM;TOR;MTB* mice (fig. S1) as well as to the primary mammary tumors arising in donor animals (*13*), and pulmonary nodules contained cells positive for MYC (Fig. 1D), keratin 8 (K8), smooth-muscle actin (SMA), and keratin 6 (K6) (fig. S2). These findings demonstrated that the tumorigenic capacity conferred on mouse mammary cells by coexpression of *MYC* and *Kras*^{D12} can be realized in the ectopic environment of the lung.

We confirmed this observation in a different mouse model, *TetO-PyMT:IRES:Luc;MMTV-rtTA* (*TOMT:IRES:Luc;MTB*), recently generated in our lab (*14*). Expression of the polyoma middle T (*PyMT*) oncogene in this line is mammary gland–specific and doxycycline-dependent and can be monitored through the coordinate expression of the reporter gene (*Luc*) encoding firefly luciferase (fig. S3). When dissociated mammary cells from mature *TOMT:IRES:Luc;MTB* animals never exposed to doxycycline were injected intravenously in *Rag1*$^{-/-}$ females on a doxycycline diet, a bioluminescence signal was apparent over the thorax of recipient mice within 2 weeks (Fig. 1E). The development of mammary tumors in the lungs of injected mice was documented by MRI imaging (Fig. 1F) and by histology (Fig. 2B). Ectopic mammary tumor foci derived from either *TOM;TOR;MTB* or *TOMT:IRES:Luc;MTB* transgenic lines displayed characteristics associated with oncogene activation at the primary site, including robust proliferation (Fig. 2C) and dense vasculature (Fig. 2D). Therefore, upon activation of potent oncogenes, previously untransformed mouse mammary cells delivered to the systemic circulation produce metastatic-like disease in the pulmonary parenchyma without having undergone transformation at the primary site.

To explore whether untransformed mammary cells can survive in the bloodstream and in the ectopic environment of the lung without oncogene expression yet still be induced to develop tumors at a later time, we injected dissociated mammary cells from *TOMT:IRES:Luc;MTB* animals never exposed to doxycycline into the lateral tail veins of *Rag1*$^{-/-}$ females on a doxycycline-free diet. No bioluminescence signal was observed in the lungs of recipient mice in up to 4 months of monitoring on this diet (Fig. 2A). When recipients were instead placed on doxycycline 1.5, 8, or 17 weeks after IV injection of transgenic mammary cells, we detected bioluminescence in the chest within 2 weeks of the start of doxycycline exposure (Fig. 2A). The histological appearance and the total number of foci in the lungs were similar in animals placed on a doxycycline diet 1 day before IV injection and 10 days after the injection [32 ± 6 (SD), $n = 5$ mice and 26 ± 6 (SD), $n = 4$ mice, respectively] (Fig. 2B). Conversion to malignancy at later times of induction was not measured because expression of the *MMTV-rtTA* transgene in the *MTB* line becomes non-uniform with age (*16*). These observations show that cells responsible for development of the ectopic mammary tumors can persist in the lung for up to 17 weeks in the absence of oncogene expression.

To rule out the possibility that low-level or transient expression of the transgenic oncogene(s) occurs in the absence of doxycycline, we carried out the modified experimental metastasis assay with mammary gland preparations from animals lacking any transgenic oncogenes (C57BL6/J mice) or from those expressing a gene encoding the "enhanced" green fluorescent protein (GFP) from the chicken β-*actin* promoter (β-*actin-GFP*) (*17*). Three weeks after the injection of mammary cells from β-*actin-GFP* mice, green foci were observed with fluorescent microscopy of the whole lungs in all recipients (Fig. 3A). These foci lacked the nodular appearance of metastatic tumors and

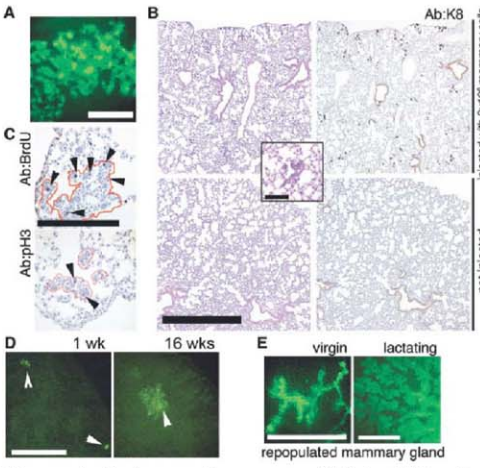

Fig. 3. Mammary cells without an oncogenic transgene can persist in the lung. **(A)** Focus of green cells observed under excitation light (*14*) in a whole fresh lung of a *Rag1*$^{-/-}$ recipient 3 weeks after IV injection of 5 × 10^5 dissociated mammary cells from a β-*actin-GFP* mouse. Scale bar, 0.1 mm. **(B)** Representative size and distribution of the H/E–stained ectopic foci in lung sections from *Rag1*$^{-/-}$ mice injected intravenously with 3 × 10^6 mammary cells from a β-*actin-GFP* donor at 3 weeks after injection (top left). Inset shows a representative H/E–stained focus at high magnification. A consecutive section (top right) was stained with rat antiserum against K8. No foci were detected by H/E (bottom left) or K8 staining (bottom right) of lung sections from uninjected *Rag1*$^{-/-}$ mice. Scale bar, 1 mm. Inset scale bar, 0.2 mm. **(C)** Mitotic activity in ectopic epithelial outgrowths (outlined in red) demonstrated by BrdU-labeling detected with rat anti-BrdU serum (arrowheads, top) or by staining with anti-pH3 (arrowheads, left). Scale bar, 0.2 mm. **(D)** Larger foci of green fluorescent cells were observed by whole-lung imaging under excitation light (*14*) at 16 weeks after injection as compared with 1 week after injection (left). *Rag1*$^{-/-}$ recipients were injected with 3 × 10^5 dissociated mammary cells from a β-*actin-GFP* mouse. Scale bar, 1 mm. **(E)** Mammary gland repopulation in secondary *Rag1*$^{-/-}$ recipients produces a green fluorescent mammary tree detectable under excitation light in the whole-mount preparations 4 or 7 weeks after transplantation (*14*). Glands were harvested from virgin recipients (left), or host animals were mated and the transplanted glands harvested 1 day postpartum (right). Scale bar, 1 mm.

were inconspicuous on routine histological inspection (Fig. 3B, top left). Staining with antibody to K8 facilitated the detection of the ectopic foci and confirmed their epithelial origin, whereas in the lungs of uninjected mice only the bronchial epithelium was stained (Fig. 3B, right).

To determine whether the ectopic foci of normal epithelial cells persist and grow in the foreign environment of the lung, we counted the total number of discrete foci in lung sections at different times after injection and looked at proliferation markers in these foci. The total number of foci found in lung sections from C57BL6/J recipients injected with 4×10^5 syngeneic mammary cells was similar in the animals surveyed at 3 weeks ($n = 3$ mice) and those surveyed at 10 weeks ($n = 3$ mice) after injection (42 ± 7 and 56 ± 22 in 10 paraffin lung sections, respectively). Moreover, the efficiency with which the wild-type cells were able to form these small epithelial clusters was similar to the efficiency with which we were able to induce ectopic tumors after injecting cells from doxycycline-naïve *TOM;TOR;MTB* donors [1.2 ± 0.4 (SD) versus 1.7 ± 1.4 (SD) per 10,000 cells injected, $n = 6$ and 8 mice, respectively; measured as described in (*14*)]. This result strongly argues that most or all of the mammary cells that are capable of surviving in the lung are able to respond to the initiating oncogene expression by forming an ectopic mammary tumor.

In both nontransgenic C57BL6/J– and β-*actin-GFP*–derived foci, occasional cells displayed mitotic activity (Fig. 3C). Consistent with this result, the green foci found under excitation light in the lungs of animals injected with mammary cells from β-*actin-GFP* mice 16 weeks after injection were larger in size than those found in recipients of the same preparation 1 week after injection (Fig. 3D). Ectopic epithelial outgrowths contained K8- and SMA-positive cells, such as observed in intact mammary glands (fig. S4A), and the outgrowths occasionally displayed a glandular appearance. Despite prolonged residence in the lung (up to 4 months), the green cells recovered from the recipients' lungs were competent to form hollow acinar structures in three-dimensional morphogenesis assays (fig. S4B) and secondary mammary outgrowths in cleared fat pads of *Rag1*$^{-/-}$ females (Fig. 3E). These findings establish that the ectopic cells residing in the lungs are indeed of mammary origin, that they are viable and mitotically active, and that at least some of them are multipotent and able to support full mammary development.

The experiments described here show that, in the absence of an active oncogene, dissociated cells from an untransformed mouse mammary gland can establish residence in the ectopic environment of the lung, grow slowly, and remain clinically undetectable after IV injection. The same cells can give rise to metastatic malignancies upon activation of oncogenes that can produce mammary tumors in an intact gland. It is widely acknowledged that multiple steps are required to establish metastases, including intravasion of cells from primary tumors into blood vessels or lymphatics; survival in the circulation, extravasation, and establishment of cells at ectopic sites; and malignant growth. Because we have injected mammary cells from transgenic mouse donors into tail veins of recipient mice, we have not examined the requirements for intravasation. We have, however, demonstrated that activated oncogenes and cellular transformation are not required for any of the subsequent steps, save for malignant growth at ectopic sites. These findings indicate that properties inherent in normal cells are sufficient for negotiating a substantial portion of the metastatic cascade. Considerable experimental and clinical evidence favors the idea that cells from small cancers may spread to distant sites early in tumorigenesis and account for dormancy and late relapse in human breast cancer (*2*, *18*). Although we do not know whether premalignant cells can enter the systemic circulation during these early stages and become sources of later metastatic tumors, our observations argue that this hypothesis should be tested. The finding that metastatic disease can arise from untransformed mammary cells in the circulation refines our conception of cancer progression, and suggests that each step in the metastatic cascade should be examined to establish its functional requirements, including those performed by normal cells. Such functions might be susceptible to inhibitory strategies that can ablate disseminated pre-malignant or malignant cells and thereby diminish the mortality caused by cancer.

References and Notes

1. D. Hanahan, R. A. Weinberg, *Cell* **100**, 57 (2000).
2. Y. Husemann *et al.*, *Cancer Cell* **13**, 58 (2008).
3. G. P. Gupta *et al.*, *Nature* **446**, 765 (2007).
4. P. B. Gupta *et al.*, *Nat. Genet.* **37**, 1047 (2005).
5. K. A. Hartwell *et al.*, *Proc. Natl. Acad. Sci. U.S.A.* **103**, 18969 (2006).
6. M. Jechlinger *et al.*, *J. Clin. Invest.* **116**, 1561 (2006).
7. R. S. Muraoka *et al.*, *J. Clin. Invest.* **109**, 1551 (2002).
8. Y. Kang *et al.*, *Cancer Cell* **3**, 537 (2003).
9. A. Muller *et al.*, *Nature* **410**, 50 (2001).
10. J. Yang *et al.*, *Cell* **117**, 927 (2004).
11. A. E. Karnoub *et al.*, *Nature* **449**, 557 (2007).
12. R. Bernards, R. A. Weinberg, *Nature* **418**, 823 (2002).
13. K. Podsypanina, K. Politi, L. J. Beverly, H. E. Varmus, *Proc. Natl. Acad. Sci. U.S.A.* **105**, 5242 (2008).
14. Materials and methods are available as supporting material on *Science* Online.
15. P. Mombaerts *et al.*, *Cell* **68**, 869 (1992).
16. E. J. Gunther *et al.*, *FASEB J.* **16**, 283 (2002).
17. M. Okabe, M. Ikawa, K. Kominami, T. Nakanishi, Y. Nishimune, *FEBS Lett.* **407**, 313 (1997).
18. J. A. Aguirre-Ghiso, *Nat. Rev. Cancer* **7**, 834 (2007).

19. We thank M. A. Melnick, G. Sanchez, A. Giannakou, and J. Demers for expert handling of the mouse colony; L. Chodosh for providing *MMTV-rtTA* transgenic mice; D. Felsher and J. M. Bishop for providing *TetO-MYC* transgenic mice; A. Olshen for assistance with statistical analysis; and L. K. Tan for assistance with histological analysis. Supported in part by awards from NIH (K01 CA118731 to K.P., P01 CA94060 to H.V., and R24 CA83084 and P30-CA 08748, which provides partial support for core facilities used in conducting this investigation), the Martell Foundation (to H.V.), and the U.S. Department of Defense (W81XWH-05-1-0220 to M.J.).

Supporting Online Material

www.sciencemag.org/cgi/content/full/321/5897/1841/DC1
Materials and Methods
Figs. S1 to S4
Table S1
References

10 June 2008; accepted 11 August 2008
10.1126/science.1161621

The Coevolution of Cultural Groups and Ingroup Favoritism

Charles Efferson,[1,2]* Rafael Lalive,[3] Ernst Fehr[1,4]

Cultural boundaries have often been the basis for discrimination, nationalism, religious wars, and genocide. Little is known, however, about how cultural groups form or the evolutionary forces behind group affiliation and ingroup favoritism. Hence, we examine these forces experimentally and show that arbitrary symbolic markers, though initially meaningless, evolve to play a key role in cultural group formation and ingroup favoritism because they enable a population of heterogeneous individuals to solve important coordination problems. This process requires that individuals differ in some critical but unobservable way and that their markers be freely and flexibly chosen. If these conditions are met, markers become accurate predictors of behavior. The resulting social environment includes strong incentives to bias interactions toward others with the same marker, and subjects accordingly show strong ingroup favoritism. When markers do not acquire meaning as accurate predictors of behavior, players show a markedly reduced taste for ingroup favoritism. Our results support the prominent evolutionary hypothesis that cultural processes can reshape the selective pressures facing individuals and so favor the evolution of behavioral traits not previously advantaged.

A cultural group is a group of people who share a set of beliefs, behavioral norms, and behavioral expectations that is recognizably different from those of other groups (*1*). Beliefs, norms, and expectations, however, are often not directly observable, and so by themselves they do not provide a practical basis for identifying cultural groups in everyday social interactions. Nonetheless, cultural groups are frequently identifiable through ethnic markers, which are arbitrary but observable traits like dress, dialect, and body modification that symbolically and conspicuously signal group affiliation (*1*–*5*).

Symbolic traits of this sort can be crucial to social and economic outcomes. When ethnic markers covary with other cultural traits, individuals can

potentially use markers to everyone's mutual advantage as indicators of what would otherwise be unobservable variation in beliefs, norms, and expectations. More nefariously, ethnic markers can lead to segregation, ethnic discrimination, and persistent inequality, even in the paradoxical cases when everyone prefers integration (*6–8*) or when ethnicity indicates nothing about competence in a given domain (*9*, *10*). Indeed, parochialism and prejudice often mar intergroup relations. People show favoritism toward ingroup members and indifference, hostility, or mistrust toward outgroup members (*11–19*). They do so even when groups are transient and group boundaries rest on the flimsiest of distinctions among individuals (*15*, *20–22*). These findings have potentially broad significance because recent theoretical research has closely and surprisingly tied outgroup hostility to the evolution of human prosociality within groups (*23*, *24*).

None of this, however, explains how a group gets to be a group and why. The long tradition of empirical research on intergroup relations (*11–22*, *25*) includes two basic approaches to defining groups. Studies have either used preexisting cultural groups, which formed beyond the ken of the studies in question, or subjects were assigned to groups exogenously as part of an experiment involving the effects of social categorization. These methods can be powerful for many questions (*12*, *16*), but they cannot expose the mechanisms behind the formation of cultural groups. These mechanisms also represent a gap in evolutionary theories of human prosociality. Although the initial evolution of cultural groups may have little to do with cooperation, much of the theory on the evolution of human prosociality relies heavily on the observation that human populations are subdivided into cultural groups (*23*, *24*, *26*). This theoretical work, however, simply imposes the required population structure exogenously. The endogenous formation of cultural groups represents a plausible route to the required population structure that figures prominently but remains unexplained in evolutionary theories of human prosociality.

We conducted a set of experiments to identify the conditions required for cultural groups to form endogenously and for subjects to show ingroup favoritism in their subsequent social interactions. We used neither preexisting cultural groups nor groups created exogenously by the experimenter. Our task instead was to see if and when symbolically marked groups form endogenously and whether their formation can lead to a preference for interactions with others having the same symbolic marker. This preference was our operational measure of ingroup favoritism in the experiment, and more generally such preferences can limit social interactions across cultural boundaries and potentially play a key role in the development of ethnocentric attitudes (*27*). If such a preference were to emerge endogenously in our setting, the result would support a central hypothesis in evolutionary social science (*27–31*). This hypothesis posits that a cultural evolutionary process can modify the selective environment facing individuals and so lead to the evolution, whether cultural or genetic, of traits that were not previously advantageous. In our case, the question is whether the evolution of cultural groups during an experiment can reconstitute the social environment to benefit ingroup favoritism in a way that did not obtain at the beginning of the experiment.

In theory, cultural groups form when variation in an unobservable but socially critical variable becomes manifest. Consider a population of players playing a simultaneous, two-person coordination game with multiple equilibria. Players can choose behavior A or B. If two players meet and choose the same behavior, a large payoff results. If they choose different behaviors (*32*), a small payoff results. Some players expect to coordinate on A, others on B. If players with different expectations meet, an information problem results. One simply has to play the odds and risk miscoordinating with someone who has incompatible expectations. This kind of problem is general. Variation in behavioral norms and expectations is widespread (*1*, *33*, *34*), and the mixing of people with different expectations occurs frequently (*1*, *35*, *36*). This mixing, however, creates the potential for people with discordant social expectations to meet, interact, and miscoordinate. Variation in expectations, however, is not enough for the existence of cultural groups because this variation is not directly observable.

Symbolic markers can change matters greatly, but only if they covary with expectations and by extension behavior. To illustrate, let players in our coordination game wear shirts with either triangles or circles. The shape on one's shirt does not affect payoffs, and so it fills the theoretical role of a symbolic marker. Consider a hypothetical population of 100 people, 50 of whom expect to coordinate on A and 50 on B. In addition, the 50 players who expect to coordinate on A have triangles on their shirts, and the 50 players who expect to coordinate on B have circles. The distribution of behavior-marker types in the population is consequently 50 (A, ▲) individuals, 0 (A, ●) individuals, 0 (B, ▲) individuals, and 50 (B, ●) individuals. The covariation between behavior and marker is at its maximum possible value in this example, and the markers perfectly reveal expectations and their associated behaviors in the coordination game. More generally, when covariation characterizes the distribution of behavior-marker types, the observable markers allow one to draw statistical inferences about what is unobservable but really important, namely, behavioral expectations in a social setting with multiple equilibria. When this is true, interacting preferentially with others having the same marker reduces the probability of miscoordination and

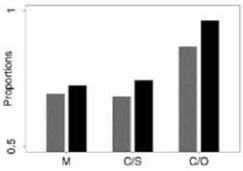

Fig. 1. Summary of linked choices for the marker-randomized (gray) and marker-maintained (black) treatments. The behavior and marker chosen in stage 1 are coded as either linked or unlinked relative to the behavior and marker chosen in stage 1 of the previous period. Proportions are plotted for the cases in which the player miscoordinated (M) in the previous period, coordinated on the suboptimal (C/S) behavior (i.e., A in subpopulation 2 or B in subpopulation 1), and coordinated on the optimal (C/O) behavior (i.e., A in subpopulation 1 or B in subpopulation 2).

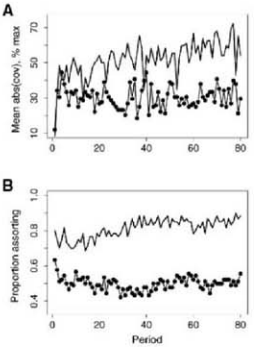

Fig. 2. (**A**) The informational content of the marker. The graph shows the mean magnitude of the covariance between behavior and marker in a subpopulation relative to the theoretical maximum for the marker-randomized (line with filled circles) and the marker-maintained (solid line) treatments. The period trend for marker-randomized is not significant [Newey-West (*40*) regression, maximal lag of 10, t test, $P = 0.368$], whereas it is highly significant for the marker-maintained treatment (Newey-West, lag of 10, t test, $P < 0.001$). (**B**) Ingroup favoritism, as indicated by the proportion of players requesting a partner with the same shape. The marker-randomized period trend is not significant (Newey-West, lag of 10, t test, $P = 0.868$). The marker-maintained period trend is highly significant (Newey-West, lag of 10, t test, $P < 0.001$), leading to large differences in ingroup favoritism across treatments.

[1]Institute for Empirical Research in Economics, University of Zürich, Blümlisalpstrasse 10, 8006 Zürich, Switzerland. [2]Santa Fe Institute, NM 87501, USA. [3]Department of Economics, University of Lausanne, 1015 Lausanne, Switzerland. [4]Collegium Helveticum, 8092 Zürich, Switzerland.

*To whom correspondence should be addressed. E-mail: efferson@iew.uzh.ch

increases expected payoffs. The puzzle, however, is how to get strong covariation endogenously in decentralized societies under limited information about the distribution of behavior-marker combinations. How does symbolic meaning emerge in the absence of fiat? Interestingly, mixing players with different expectations, which creates the original problem, also creates a potential solution. It does so by producing small amounts of covariation (*37*) that can feed back into the system and accumulate dynamically (*38, 39*).

The accumulation of covariation requires more than mixing, however, because mixing by itself often creates only a small amount of covariation between behavior and marker (*38*). During our experiment, individuals did not have information about the aggregate distribution of behavior-marker combinations, and thus it would have been difficult or impossible to recognize an initially weak relation between behavior and marker. Covariation can increase, however, if individuals link behaviors and markers in specific ways. Linkage refers to a tendency for an individual either to retain both her current behavior and marker or to change both her behavior and marker; what an individual does not do is change one trait but not the other. Linkage is crucial because it preserves the covariation created by earlier mixing, while continued mixing creates additional covariation that feeds back into the system and gets added to existing covariation. The result is that the total covariation accumulates, and this increases the economic incentives to interact with others having the same marker. For covariation to accumulate, however, linkage should not be indiscriminate. Rather, theory suggests it should be more prevalent in specific situations like those in which individuals acquire information about economically successful behavior-marker combinations (*38, 39*). If individuals, however, never link under any circumstances because they choose behaviors and markers independently, covariation is constantly destroyed, and markers cannot become strongly associated with behavior.

We conducted the following experiment to see if players would show a preference for (i) linking behaviors and markers and for (ii) interacting with partners displaying the same marker. In addition, we wanted to know (iii) whether linkage, if present, would generate sizable covariation between behavior and marker, which would then enable subjects to increase coordination via ingroup favoritism. Players were assigned to one of multiple populations of 10. We randomly subdivided these 10 players into two subpopulations of 5. Players within a subpopulation played one of two coordination games (table S1). Each game had two pure-strategy equilibria, and thus players had to solve a coordination problem. Both games had two behaviors to choose from, A and B, but in subpopulation 1, coordinating on A (41 points for each player paired with another playing A) was better than coordinating on B (21 points for each player paired with another playing B), whereas in subpopulation 2, coordinating on B (41 points) was better than coordinating on A (21 points). Miscoordinating in either subpopulation brought a small payoff (1 point). Payoffs were designed to draw players in different subpopulations toward different behaviors and so mimic the variation in norms, preferences, and expectations that often exists because of historical separation or important but unobservable environmental differences.

To create a persistent coordination problem, players from the different subpopulations were mixed, and they were never told to which subpopulation they were assigned. If players had remained in their initial subpopulations, the game would have posed little problem. Players would have soon figured out their respective situations, and presumably players in subpopulation 1 would have only chosen A, whereas players in subpopulation 2 would have only chosen B. Each period, however, a randomly selected player from subpopulation 1 and a randomly selected player from subpopulation 2 switched subpopulations. All players knew this would happen, but no one knew which two players had switched. In sum, each player had a strong incentive to develop accurate expectations about her current subpopulation, but from time to time she found herself in a new situation where her social expectations ran askew of local norms.

Players could also condition social interactions on symbolic markers. In each period, each player chose one of two shapes, ▲ or ●. A player's payoff did not directly depend on her shape, but players could use shapes to influence with whom they would play the coordination game (*39*). The experiment lasted 80 periods. Each period proceeded as follows.

Stage 1. Each player chose a payoff-relevant behavior, A or B, for the coordination game and a payoff-irrelevant shape, ▲ or ●.

Stage 2. An unidentified player from each subpopulation switched subpopulations.

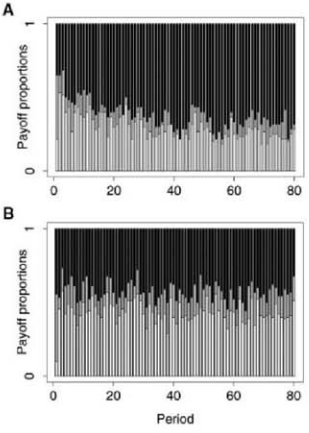

Fig. 3. Payoff proportions in the marker-maintained treatment (**A**) and the marker-randomized treatment (**B**). The graphs show the distribution of players by period coordinating on the optimal behavior (black) given the subpopulation (A in 1, B in 2), coordinating on the suboptimal behavior (gray) given the subpopulation (A in 2, B in 1), or miscoordinating (white). See supporting online text for a multinomial regression analysis.

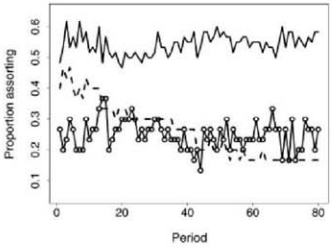

Fig. 4. Ingroup favoritism for the modified marker-maintained (solid line), payoff-equivalent (dashed line), and fixed-marker (line with open circles) treatments. Newey-West (*40*) regressions indicate that the modified marker-maintained treatment began with more assortment than the other two treatments, and the differences across treatments increased through time. Comparison of regression results for the modified marker-maintained and payoff-equivalent treatments shows that the intercepts are significantly different (z test, $P < 0.001$), as are the period trends (z test, $P < 0.001$). Comparison of results for modified marker-maintained and fixed-marker shows that both the intercepts (z test, $P < 0.001$) and period trends (z test, $P = 0.019$) are significantly different.

Stage 3. Each player indicated whether she wanted to play the coordination game with (i) a randomly selected player with the same shape from her subpopulation or (ii) any randomly selected player from her subpopulation.

Stage 4. Each player was paired using her choice in stage 3 and received a payoff based on her behavior, her partner's behavior, and their subpopulation.

To clarify our discussion of the results, when there was little or no covariation between behavior and marker, we will call a set of individuals who shared the same marker a "trivial" group. These groups were trivial in the sense that the markers partitioned the population into circles and triangles, but these markers did not reliably reflect any underlying variables affecting payoffs. We will call a group "cultural," in contrast, only when a set of individuals shared the same marker after a sustained increase in the aggregate covariation between behavior and marker. Groups were cultural in this case because markers did not simply partition the population into circles and triangles; they also, on average, partitioned the population into those who expected to coordinate on A versus those who expected to coordinate on B.

The experiment consisted of two treatments. In the marker-randomized treatment, each player was randomly assigned a shape after stage 2 regardless of the shape chosen in stage 1. In the marker-maintained treatment, each player retained her chosen shape. The marker-randomized treatment was a control treatment in which marker randomization precluded the possibility of the marker becoming an accurate predictor of behavior. The comparison between the two treatments shows (i) how much informational content the marker acquired in the marker-maintained treatment beyond the baseline when markers were randomly assigned and (ii) whether any differences in informational content translated into differences in the preference for ingroup favoritism.

Subpopulations were not equivalent to symbolically marked groups, whether trivial or cultural. In a given period, a player's subpopulation was the pool of players available for social interaction. A symbolically marked group, in contrast, was the set of players from the entire population with the same marker. In short, the division of players into two subpopulations, one favoring behavior A and the other behavior B, sustained variation in norms and expectations. This variation, however, was not observable, and so it could not by itself serve as a means of distinguishing one group from another. Symbolic markers, in contrast, were observable traits, and they could serve as a means of distinguishing one group from another. Markers, however, did not bear any necessary relation to behavior and subpopulation. The significance of markers, in essence, could only emerge during the experiment as a result of player choices. Markers had the potential to become the basis for determining cultural group affiliation ex post, and indeed that was our question, but they were devoid of content ex ante.

For a sustained increase in covariation, individuals have to link the behavioral and marker dimensions. We coded behavior-marker choices from stage 1 of periods 2 to 80 as "linked" or "unlinked." A linked choice was one in which a player either retained her behavior and chosen marker from the previous period or changed both. An unlinked choice was when she changed her behavior or marker but not both. A strong preference toward linked choices was present in general (Fig. 1), but it was significantly stronger in the specific case when a player received the optimal coordination payoff in the previous period (conditional logit, $P < 0.001$, table S3). These linked choices consisted almost exclusively of choices in which the player retained her behavior and marker from the previous period (figs. S1 and S2). In addition, although the preference for linked choices after coordinating on the optimal behavior was present in both treatments, it was significantly stronger in the marker-maintained treatment (conditional logit, $P < 0.001$, table S3). These results indicate that players showed a general tendency to couple behaviors and markers. This tendency, however, was strongest when a player hit upon a successful behavior-marker combination, and it was further reinforced and amplified in the marker-maintained treatment when the marker was not prevented from acquiring meaning.

Substantial linkage at the individual level produces covariation between behavior and marker at the aggregate level. If strong enough and specific enough, the linkage exhibited in the experiment should have produced a significant increase in covariation in the marker-maintained treatment, when it was possible, but not in the marker-randomized treatment, when it was not. Even though linkage was present, however, covariation should have been similar in the two treatments at the beginning of the experiment, before covariation had time to accumulate. Only in later periods should the covariation have been significantly higher in the marker-maintained treatment. The aggregate covariation between behavior and marker indeed followed this dynamical pattern. During the first five periods, the covariation was not different in the two treatments (Welch two-sample t test, df = 7.01, two-sided $P = 0.68$, Fig. 2A), whereas in the final five periods, the covariation was significantly higher in the marker-maintained case (Welch two-sample t test, df = 12.107, two-sided $P < 0.001$, Fig. 2A). Covariation thus strongly and significantly increased in the marker-maintained treatment but not in the marker-randomized case. This led to a strong overall treatment difference in the accumulation of the markers' predictive power [Newey-West regression (*40*), $P < 0.001$, Fig. 2A].

The presence of covariation does not mean that players will exploit it by assorting into groups characterized by shared markers. Players could simply fail to recognize the association between behavior and marker as it developed, or they could fail to recognize its usefulness. Nonetheless, players exhibited an increasing inclination to request partners with the same shape as covariation accumulated. Throughout the marker-randomized treatment, players requested same-shape partners roughly 50% of the time (Fig. 2B), a result consistent with indifference concerning the two interaction policies. In the marker-maintained treatment, however, players increasingly requested partners having the same shape as time passed. This increase was highly significant (Newey-West regression, $P < 0.001$), and the vast majority of players (87%) requested partners with the same shape in the final five periods (Fig. 2B), indicating that ingroup favoritism became an almost universal phenomenon.

In the presence of covariation, this kind of ingroup favoritism should lead to more coordination and improved payoffs, but the strength of the effect will vary with the degree of covariation and preferential assortment. A calculation of the mean payoff over periods for each subject shows that payoffs were significantly different across the two treatments. The mean payoff in the marker-randomized treatment was 20.819 points, and it was 27.454 in the marker-maintained treatment (Welch two-sample t-test, df = 88.912, two-sided $P < 0.001$). This difference, however, depended specifically on the dynamical increase in the markers' predictive content in the marker-maintained treatment, and this fact is central to our finding that the evolution of cultural groups changed the incentives associated with ingroup favoritism. Specifically, for those players who requested a partner with the same shape, the mean payoff per period was not significantly different between the two treatments in the first five periods (Welch two-sample t-test, df = 123.139, two-sided $P = 0.1638$), whereas it was highly significant in the final five periods (Welch two-sample t test, df = 105.733, two-sided $P < 0.001$). The higher overall payoffs in the marker-maintained treatment stemmed from an increase in coordinating on the optimal behavior in each of the two subpopulations (Fig. 3). A detailed analysis formally confirms the substantial and robust payoff effect that resulted from assorting on markers in the marker-maintained treatment (*37*).

These results show how the evolution of cultural groups can reconstitute the social environment and produce selection for an ingroup bias that was not initially advantageous. If selective pressures of this sort were common in past human societies, a plausible outcome would arguably be a relatively inflexible bias leading individuals to prefer others similar in some symbolic dimension. This idea is consistent with much research showing an astonishing willingness for subjects to exhibit ingroup favoritism when groups are based on trivial, short-lived distinctions (*12*, *15*, *16*, *21*, *22*). For our study, this could mean that the marker-based assortment we documented largely reflected a readiness to favor the ingroup that was already in place when the subjects came to the lab, and it did not stem from the endogenous formation of cultural groups during the experiment. In particular, although we found a pronounced difference in assortment dynamics in our two treatments, we still found a strong tendency to assort in the marker-randomized treatment. This assortment was relatively meaningless with respect to payoffs, but

because requesting a partner with the same shape was free, it is consistent with two different motives on the part of players. Players could have simply been indifferent between two largely meaningless, cost-free social interaction policies, or they could have had a strong residual taste for same-shape partners even when such pairings did not improve payoffs. To distinguish between these two possibilities, we conducted a second experiment with three treatments, all of which required subjects to pay a small cost for ingroup favoritism.

In the three treatments of our second experiment (*37*), subjects had to pay a cost of 1 point when they requested and were successfully paired with a partner having the same shape. To maximize the salience of the marker, all players retained their chosen markers in all treatments. In the payoff-equivalent treatment, the payoff structure was changed such that coordinating on A or B yielded the same payoff (21 points) regardless of the players' subpopulation. Because the payoff structure in the subpopulations was identical in this case, players did not differ in terms of some unobservable variable related to payoffs, and thus they had no material problem the markers could help them solve. They could, of course, continue to bias their interactions toward those having the same marker if willing to pay the cost. In the fixed-marker treatment, players only chose a marker in the first period. This marker was then retained for all 80 periods. In this treatment, markers were ostensibly similar to traits like race that are often perceived as immutable. Because of this perceived immutability, which may or may not be an accurate perception, such traits are especially prone to essentialist generalizations and are thus prime candidates for generating ingroup favoritism and outgroup hostility (*41*). A truly immutable marker, however, like the one we implemented, should not evolve to be a stable predictor of behavior because individuals cannot adjust their markers to reflect changing social circumstances. In the fixed-marker treatment, for example, players could benefit from changing their expectations about where to coordinate when they changed subpopulations, but they could not change their markers to signal their shifting expectations. Players could nonetheless choose to assort on marker, if they wished. Lastly, as a new baseline, the modified marker-maintained treatment was similar to the original marker-maintained treatment, but it involved the same assortment cost used in the payoff-equivalent and fixed-marker cases.

As in the original marker-maintained treatment, the covariance between behavior and marker accumulated at a significant rate through time in the modified marker-maintained treatment [Newey-West (*40*) regression, maximal lag of 10, period trend t test, $P = 0.003$]. In early periods, the covariance in the fixed-marker treatment was lower than it was in the modified marker-maintained treatment, and this difference was marginally significant (z test on Newey-West estimated intercepts, $P = 0.067$). Furthermore, unlike the modified marker-maintained case, covariation did not accumulate through time in the fixed-marker treatment (Newey-West regression, lag of 10, period trend t-test, $P = 0.294$). The estimated time trend was slightly negative, and this was significantly different from the positive trend in the modified marker-maintained treatment (z test on Newey-West estimated period coefficients, $P = 0.002$). In the payoff-equivalent treatment, covariance was significantly lower in early periods than it was in the modified marker-maintained treatment (z-test on Newey-West estimated intercepts, $P < 0.001$), and it declined even further at a significant rate (Newey-West regression, lag of 10, period trend t test, $P < 0.001$). In this case, covariance actually declined all the way to 0 because all players soon converged on A in all subpopulations. With no variation in behavior, covariation between behavior and marker is not possible. Shared history was sufficient to form accurate expectations about where to coordinate, and the marker was not useful in this respect. In sum, trivial groups became cultural groups in the modified marker-maintained treatment, but trivial groups remained trivial in the payoff-equivalent and fixed-marker treatments.

Players, in turn, responded strongly to the resulting variation in the accumulated predictive power of markers. In the modified marker-maintained baseline, roughly 55 to 60% of the players requested partners with the same shape in later periods (Fig. 4). In the payoff-equivalent and fixed-marker treatments, however, only 15 to 25% assorted on shape in later periods, and the differences relative to the baseline were highly significant (Fig. 4). The payoff-equivalent case is especially clear because, as mentioned above, all players eventually played A in both subpopulations, and the predictive value of the markers went to zero as a result. Correspondingly, the proportion of players requesting same-shape partners unraveled relentlessly as the experiment progressed (Fig. 4). The fact that assortment did not disappear altogether suggests that perhaps a few players had a weak taste for assortment even when this did not improve coordination. Altogether, however, our results show that the preference for interacting with similarly marked players varied strongly according to whether markers became accurate predictors of behavior in the face of heterogeneous behavioral expectations. In short, ingroup favoritism had little to do with an unconditional preference for similarly marked partners and a lot to do with whether trivial groups evolved into cultural groups. For this cultural evolutionary transition to happen, two requirements had to be met. First, players had to differ persistently in some important but unobservable dimension that could sustain symbolic representation. Our payoff-equivalent treatment removed this feature, and assorting on shape steadily declined through time. Second, the symbolic markers themselves had to be freely chosen and mutable in a way that allowed an association between markers and unobservables to develop. Our marker-randomized and fixed-marker treatments removed this feature, and assorting on shape was relatively low in all periods when compared to their respective marker-maintained treatments.

The research on intergroup processes indicates that people have a willingness to show ingroup favoritism, and in particular this holds even when groups are trivial and evanescent (*12*, *13*, *16*–*18*, *20*–*22*, *25*). This research tradition has generally examined neither the evolutionary mechanisms behind group formation nor the impact of these mechanisms on ingroup favoritism. We implemented an experiment in which the significance of groups had to arise, if at all, endogenously, thus providing an evolutionary foundation for ingroup favoritism. In this setting, trivial groups remained trivial under certain circumstances, but under other circumstances they developed into cultural groups composed of individuals who shared both behavioral expectations and symbolic markers signaling group affiliation. Ingroup favoritism was strongly associated with cultural groups but not with trivial groups. Our experiments made exclusive use of coordination games, which serve as a kind of generic proxy for strategic settings with multiple equilibria. Many strategic settings are characterized by multiple equilibria (*42*), and thus the dynamical processes examined here have potentially broad significance. The mechanisms implicated in the evolution of human prosociality, for example, often produce multiple equilibria (*43*, *44*), and so cooperation is a behavioral domain with considerable scope for the path-dependent evolution of groups with different norms and expectations. In this sense, cooperation can be analogous to coordination. Even more generally, whenever people have a shared interest in distinguishing among themselves in terms of their unobservable information (*38*), whatever that means in a given situation, the logic behind the evolution of cultural groups holds.

References and Notes

1. F. Barth, Ed., *Ethnic Groups and Boundaries: The Social Organization of Cultural Difference* (Little, Brown, Boston, 1969).
2. D. E. Blom, *J. Anthropol. Archaeol.* **24**, 1 (2005).
3. J. B. Eicher, Ed., *Dress and Ethnicity: Change Across Space and Time* (Berg, Oxford, 1995).
4. C. Silverman, *J. Am. Folkl.* **101**, 261 (1988).
5. C. Torres-Rouff, *Curr. Anthropol.* **43**, 163 (2002).
6. S. Bowles, *Microeconomics: Behavior, Institutions, and Evolution* (Russell Sage, New York, 2004).
7. T. Schelling, *Micromotives and Macrobehavior* (Norton, New York, 1978).
8. H. P. Young, *Individual Strategy and Social Structure: An Evolutionary Theory of Institutions* (Princeton Univ. Press, Princeton, NJ, 1998).
9. R. L. Axtell, J. M. Epstein, H. P. Young, in *Social Dynamics*, S. N. Durlauf, H. P. Young, Eds. (MIT Press, Cambridge, MA, 2001), pp. 191–211.
10. S. Bowles, G. Loury, R. Sethi, "Is equal opportunity enough? A theory of persistent group inequality," Santa Fe Institute Working Paper; www.santafe.edu/~bowles.
11. H. Bernhard, U. Fischbacher, E. Fehr, *Nature* **442**, 912 (2006).
12. J. F. Dovidio, P. Glick, L. A. Rudman, Eds., *On the Nature of Prejudice: Fifty Years After Allport* (Blackwell, Oxford, 2005).
13. R. H. Fazio, J. R. Jackson, B. C. Dunton, C. J. Williams, *J. Pers. Soc. Psychol.* **69**, 1013 (1995).
14. E. L. Glaeser, D. I. Laibson, J. A. Scheinkman, C. L. Soutter, *Q. J. Econ.* **115**, 811 (2000).
15. L. Goette, D. Huffman, S. Meier, *Am. Econ. Rev.* **96**, 212 (2006).

16. M. Hewstone, M. Rubin, H. Willis, *Annu. Rev. Psychol.* **53**, 575 (2002).
17. K. D. Kinzler, E. Dupoux, E. S. Spelke, *Proc. Natl. Acad. Sci. U.S.A.* **104**, 12577 (2007).
18. Z. Kunda, *Social Cognition: Making Sense of People* (MIT Press, Cambridge, MA, 1999).
19. T. Yamagishi, N. Jin, T. Kiyonari, *Adv. Group Process.* **16**, 161 (1999).
20. M. B. Brewer, *Pers. Soc. Psychol. Bull.* **17**, 475 (1991).
21. M. Sherif, O. J. Harvey, B. J. White, W. R. Hood, C. W. Sherif, *Intergroup Conflict and Cooperation: The Robbers Cave Experiment* (Institute of Group Relations, Univ. of Oklahoma, Norman, OK, 1961).
22. H. Tajfel, M. G. Billig, R. P. Bundy, C. Flament, *Eur. J. Soc. Psychol.* **1**, 149 (1971).
23. R. Boyd, H. Gintis, S. Bowles, P. J. Richerson, *Proc. Natl. Acad. Sci. U.S.A.* **100**, 3531 (2003).
24. J.-K. Choi, S. Bowles, *Science* **318**, 636 (2007).
25. J. Correll, G. R. Urland, T. A. Ito, *J. Exp. Soc. Psychol.* **42**, 120 (2006).
26. R. Boyd, P. J. Richerson, *J. Theor. Biol.* **215**, 287 (2002).
27. R. Boyd, P. J. Richerson, *The Origin and Evolution of Cultures* (Oxford Univ. Press, Oxford, 2005).
28. R. Boyd, P. J. Richerson, *Culture and the Evolutionary Process* (Univ. of Chicago Press, Chicago, 1985).
29. W. H. Durham, Ed., *Coevolution: Genes, Culture, and Human Diversity* (Stanford Univ. Press, Stanford, CA, 1991).
30. F. J. Olding-Smee, K. N. Laland, M. W. Feldman, *Niche Construction: The Neglected Process in Evolution* (Princeton Univ. Press, Princeton, NJ, 2003).
31. P. J. Richerson, R. Boyd, *Not By Genes Alone: How Culture Transformed the Evolutionary Process* (Univ. of Chicago Press, Chicago, 2005).
32. It is not crucial for our purposes that identical actions lead to high payoffs. Instead, the necessity of coordinated choices for a high payoff is important. Thus, if the choice combination A for player 1 and B for player 2 led to a high payoff, then the players would simply need to coordinate on (A, B). Almost every bargaining problem or economic exchange involves some necessity for coordinating expectations and actions.
33. J. G. Jorgensen, *Western Indians* (Freeman, New York, 1980).
34. C. M. Judd, B. Park, in *On the Nature of Prejudice: Fifty Years After Allport*, J. F. Dovidio, P. Glick, L. A. Rudman, Eds. (Blackwell, Oxford, 2005), pp. 123–138.
35. S. Bowles, *Science* **314**, 1569 (2006).
36. R. F. Heizer, in *Handbook of North American Indians: California*, R. F. Heizer, W. C. Sturtevant, Eds. (Smithsonian Institution, Washington, DC, 1978), pp. 690–693.
37. Materials and methods are available as supporting material on *Science* Online.
38. R. Boyd, P. J. Richerson, *Cult. Anthropol.* **2**, 65 (1987).
39. R. McElreath, R. Boyd, P. J. Richerson, *Curr. Anthropol.* **44**, 122 (2003).
40. W. K. Newey, K. D. West, *Econometrica* **55**, 703 (1987).
41. J. T. Jost, D. L. Hamilton, in *On the Nature of Prejudice: Fifty Years After Allport*, J. F. Dovidio, P. Glick, L. A. Rudman, Eds. (Blackwell, Oxford, 2005), pp. 208–224.
42. D. Fudenberg, E. Maskin, *Econometrica* **54**, 533 (1986).
43. R. Boyd, P. J. Richerson, *Ethol. Sociobiol.* **13**, 171 (1992).
44. K. Panchanathan, R. Boyd, *Nature* **432**, 499 (2004).
45. This research was supported by the Swiss National Science Foundation (105312-114107) and is part of the Research Priority Program "Foundations of Human Social Behavior—Altruism versus Egoism" at the University of Zurich. We thank S. Bowles for valuable comments on an earlier version of this article and R. McElreath for helpful insights during the initial stages of the project.

Supporting Online Material

www.sciencemag.org/cgi/content/full/321/5897/1844/DC1
Materials and Methods
SOM Text
Figs. S1 and S2
Tables S1 to S10
References

29 January 2008; accepted 20 August 2008
10.1126/science.1155805

Understanding Overbidding: Using the Neural Circuitry of Reward to Design Economic Auctions

Mauricio R. Delgado,[1] Andrew Schotter,[2] Erkut Y. Ozbay,[3] Elizabeth A. Phelps[4]*

We take advantage of our knowledge of the neural circuitry of reward to investigate a puzzling economic phenomenon: Why do people overbid in auctions? Using functional magnetic resonance imaging (fMRI), we observed that the social competition inherent in an auction results in a more pronounced blood oxygen level–dependent (BOLD) response to loss in the striatum, with greater overbidding correlated with the magnitude of this response. Leveraging these neuroimaging results, we design a behavioral experiment that demonstrates that framing an experimental auction to emphasize loss increases overbidding. These results highlight a role for the contemplation of loss in understanding the tendency to bid "too high." Current economic theories suggest overbidding may result from either "joy of winning" or risk aversion. By combining neuroeconomic and behavioral economic techniques, we find that another factor, namely loss contemplation in a social context, may mediate overbidding in auctions.

An unresolved question in the emerging field of neuroeconomics is whether data from neuroscience can inform economic theory such that it motivates behavioral economic institutional design (*1*–*4*). In this report, we address this question by taking advantage of our knowledge of the neural circuitry of reward to investigate a puzzling economic phenomenon. Specifically, why do people overbid in auctions? (*5*, *6*).

Auctions are an old and widely used method in allocating goods (*7*). Mention of them dates back to Roman times, when spoils of war were sold on the block. Although there are many different types of auctions, they all share the feature that bidders must determine a bidding strategy (or bid function) to be used in submitting their bid. A bid function for a buyer in an auction is a mapping from the value that the bidder places on the good for sale to the bid chosen. A set of bidding functions is considered to be an equilibrium (Nash equilibrium) if, given the strategy used by one's opponents, no bidder has any incentive to change his or her bidding strategy. One robust finding in experimental auctions is that bidders tend to bid above their Nash equilibrium risk-neutral bid function (*5*); this behavior has been labeled "overbidding" in the economics literature. In other words, given the value of the good for sale they submit bids that are "too high." Two competing explanations for this phenomenon exist. Many scholars have assumed that risk aversion is responsible for this increase in bids, because bidding above one's risk-neutral Nash equilibrium bid function is exactly what risk aversion prescribes (*5*, *6*, *8*). Another explanation stems from the ideas that bidders enjoy a "joy of winning" the social competition inherent in an auction (*5*, *6*).

The goal of this study is to provide insight into the neural circuitry of experimental auctions and to use this insight to generate and test a behavioral economic approach to understand overbidding. First, we used functional magnetic resonance imaging (fMRI) to examine the neural correlates of winning and losing an experimental auction, while modulating potentially important variables such as type of social competition (auction versus lottery) and type of incentive (money versus points with no monetary value). On the basis of these brain imaging results and our understanding of the neural circuitry of reward, we generated a hypothesis concerning the mechanisms underlying overbidding in experimental auctions. We then tested this hypothesis in a behavioral economic experiment.

In the fMRI study, 17 participants were instructed that they would each be playing two types of games: a two-person auction and a lottery (52 events for each treatment) (*9*). Before participants were scanned, they briefly met their competitor for the auction and were informed that they would be playing an unknown but fixed strategy. In the auction game, participants were assigned a value (V) at the beginning of each trial. These values were drawn from a finite set with equal probability. Participants were asked to choose a bid (b) (the decision phase) and were then informed if they won or lost the auction (the outcome phase). There were four possible V's assigned for the good sold (6, 8, 10, 12) and four options for b (2, 5, 7, 8). The competitor bid according to the Nash equilibrium strategy (V:b equals 6:2, 8:5, 10:7, 12:8). In the money condition, V and b represented dollars, and the participants were informed they would receive a payoff of V minus b if they won that trial and zero if they lost. They would be paid their total winnings from one randomly selected block out of the four

[1]Department of Psychology, Rutgers University, Newark, NJ 07102, USA. [2]Department of Economics, New York University, and Center for Experimental Social Science, New York, NY 10003, USA. [3]Department of Economics, University of Maryland, College Park, MD 20742, USA. [4]Department of Psychology, New York University, New York, NY 10003, USA.
*To whom correspondence should be addressed. E-mail: liz.phelps@nyu.edu

money blocks presented (each encompassing 13 trials) at the end of the study. In the points condition, V and b represented points. Participants were told that the accumulation of points from a random points block (the sum of V minus b for win trials) would be a measure of how well they did relative to other participants, with final anonymous results disseminated at the conclusion of the study. The auction game used the first-price sealed-bid rule in which the participant did not know the V assigned to the competitor on each trial and the higher bid won. In case of identical bids, ties were broken at random. Because losses yielded zero payoffs, a loss did not signify a monetary or points loss per se, but merely that the participant did not win that particular auction (*10*).

In the lottery game, subjects played against a computer that used the same fixed Nash equilibrium bid strategy as the auction game confederate. Unlike the auction, participants were not required to submit a bid for the random value assigned to them. Rather, they were assigned both V and b at the beginning of each trial and were simply asked to indicate if they wanted to play the lottery for that trial (decision phase). If their assigned b was greater than the b generated by the computer's Nash equilibrium bid, they won the lottery, if not, they lost (outcome phase). As in the auction game, participants played the lottery for either money or points. Behavioral measures of reaction time and choice were collected throughout the experiment, along with postexperimental Likert-scale ratings (*9*).

As in previous auction studies (*5*, *6*), participants overbid with respect to the risk-neutral Nash equilibrium [$t(16) = 3.04$, $P < 0.008$]. Overbidding compared with choosing the equilibrium bid was greatest when the incentive was monetary [$t(16) = 3.30$ $P < 0.005$]. Overall, participants' chosen b was greater than the equilibrium b on 65% of the money trials and 57% of the point trials (*11*).

The goal of the fMRI study was to examine the effects of type of social competition (auction versus lottery) and type of incentive (money versus points) on blood oxygen level–dependent (BOLD) responses to winning or losing. Given this, the focus of the analysis was the outcome phase. Statistical maps contrasting wins and losses across all conditions were generated ($P < 0.001$, cluster threshold of 3 mm^3 contiguous voxels). Mean beta weights (*19*) from each region of interest (ROI) defined by this contrast were extracted and input into two separate analyses of variance (ANOVAs) to examine main effects of social competition and incentive during win or loss outcomes separately. Regions identified during the outcome phase included both left and right striatum, specifically the ventral caudate nucleus, previously implicated in monetary outcome processing and learning from feedback (*12*–*18*), along with ROIs in the occipital lobe (table S4). An examination of the BOLD response in these ROIs revealed differential responses for type of social competition or for type of incentive, only in the right and left striatum (Fig. 1A). Activation in this region has previously been shown to be graded according to the magnitude of monetary gain and loss during probabilistic games (*12*–*15*), with an increase in BOLD signal relative to resting baseline for positive outcomes (wins) and a decrease for negative outcomes (losses) (*14*–*16*) that resemble learning signals (*17*, *18*). Within the right striatum ROI (*20*), results differed across win and loss trials. A main effect of incentive ($F_{1,16} = 9.67$, $P < 0.01$) was observed during win trials, driven primarily by a larger response to monetary reward compared with points reward [$t(16) = 3.11$, $P < 0.01$], but no main effect of social competition was observed. Instead, differences between auction and lottery trials were apparent only in the context of losses ($F_{1,16} = 5.29$, $P < 0.05$). Of particular interest, post hoc t tests showed that mean beta weights for win trials during the auction game (irrespective of incentive) were not significantly different from the lottery game [$t(16) = -0.60$, $P = 0.55$]. In contrast, mean beta weights for losses led to a more pronounced decrease from baseline

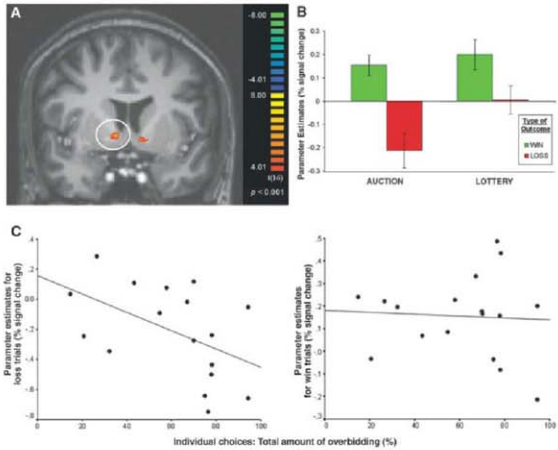

Fig. 1. Striatal response to loss is enhanced by social competition in the auction game. **(A)** Win versus loss outcome contrast: right striatum, including the ventral caudate nucleus was identified as a region of interest (peak at $x, y, z = 10, 2, 1$). **(B)** Parameter estimates, or mean beta weights, for win and loss trials from the right ventral caudate ROI for auction and lottery games show differential responses between auction and lottery only during losses. Error bars are SEM. **(C)** Across participants, the general tendency to overbid during auction trials correlated with BOLD signals in the right striatum ROI (depicted by parameter estimates) when an auction outcome was a loss ($r = -0.493$, $P < 0.05$), but not when the outcome was a win ($r = -0.059$, $P = 0.82$).

Table 1. Results of two separate regressions on the auction data (cluster analysis by subjects) (±SEM). First regression analysis: Overbids are regressed on BOLD signals from the right striatal ROI for individual win-and-loss trials (outcome phase) during the auction game. Second regression analysis: Overbids are regressed on BOLD signals from the rights striatum ROI and on values (V). The number of observations (N) for each trial is given.

Type of trial	N	Regression coefficient	
		Values	BOLD Signal
		First regression analysis	
Win trials	397		−0.016 ± 0.1342
Loss trials	372		−0.316 ± 0.2384*
		Second regression analysis	
Win trials	397	0.024 ± 0.0208*	−0.04 ± 0.1249
Loss trials	372	0.072 ± 0.0816	−0.237 ± 0.1836*

*$P < 0.05$

during auction compared with lottery trials [$t(16) = -2.30$, $P < 0.05$; (Fig. 1B)]. Finally, a correlation between mean beta weights in the right striatal ROI and a participant's tendency to overbid in general (i.e., the total number of times a participant chose to overbid during auction trials) was observed for loss ($r = -0.493$, $P < 0.05$), but not win ($r = -0.059$, $P = 0.82$) outcomes (Fig. 1C).

Given that there was no actual loss of money or points in either game, it is somewhat surprising that the response to losses during the auction game yielded a significant decrease in BOLD signal relative to the resting baseline and the lottery game. One possibility is that the social competition inherent in the auction game resulted in a loss signal in the right striatum, mirroring that observed with actual monetary loss. The importance of social competition in driving responses in the auction game is further supported by the data from the points condition. Notably, the points incentive could be interpreted as a more relative reward (with respect to other competitors), whereas the monetary incentive is a more abstract reward. A two-way repeated measures ANOVA, including only the data from the points condition with type of social competition and type of feedback (win and loss) as factors, revealed a main effect of competition ($F_{1,16} = 4.44$, $P < 0.05$). This was driven by right striatal responses to winning versus losing during the auction [$t(16) = 2.01$, $P = 0.06$], rather than the lottery game [$t(16) = 0.50$, $P = 0.63$] (see fig. S1). The finding that social factors can modulate responses in the striatum to monetary incentives has been previously demonstrated with other economic games (*21*–*25*). For experimental auctions, it appears that the social interaction specifically alters the response to losses in the striatum, in addition to enhancing overall responses to a nonmonetary reinforcer.

Although the inference of psychological states from BOLD responses should generally be viewed with caution (*26*), our imaging results provide some initial hypotheses as to the nature of overbidding in experimental auctions. The lack of an enhanced BOLD response in the striatum to wins (in the auction compared with the lottery) suggests that the "joy of winning" may not be mediating overbidding in experimental auctions. In contrast, the stronger BOLD response to losses in the auction game suggests that a fear of losing a social competition may be linked to overbidding. The fear of losing the social competition of an auction may lead to a striatal response similar to that observed in loss aversion (*27*). However, because no actual losses occurred in this experiment, it would appear that the "fear of losing" the social competition was a factor independent of pure loss aversion.

To further explore these hypotheses a post hoc analysis was conducted. For each subject, we extracted beta weights from the right striatal ROI for wins and losses (outcome phase) for each auction trial. With these beta values, we ran two separate regressions, with a cluster analysis by subjects, examining the relation between the overbids (the difference between the actual bids and the Nash equilibrium), the value assigned (V), and the BOLD response during the outcome phase to a win or loss. Our results indicate that the BOLD response coefficient is not significantly different than 0 for the win trials [$t = -0.25$, $P > 0.05$], but significant responses are observed for loss trials ($t = -2.81$, $P < 0.05$) (Table 1, first regression analysis). The BOLD response regression coefficient of loss trials is significant even when value (V) is included as a controlling factor ($t = -2.74$, $P < 0.05$) (Table 1, second regression analysis). These results, combined with our cross-subject correlation (see Fig. 1C), lead to the intriguing conjecture that perhaps it is the anticipation of a possible loss in experimental auctions that is, at least in part, driving the tendency to bid "too high."

If this conjecture is correct, we should be able to take advantage of this fear of losing to design an experimental auction that will result in an even stronger tendency to overbid. More precisely, if the anticipation of the unpleasant state associated with loss led participants to increase their bids to avoid that state, then manipulating the parameters of a first-price auction to highlight the potential for loss, as opposed to gain, should increase bid values, even if the equilibrium bid function was left unaltered. Hence, we would expect that the loss-frame auction would not only increase bids conditional on value, but also raise more revenue than either a control auction or one where gains or "wins" are emphasized.

In order to test these assumptions, we ran a behavioral economic experiment with three conditions. In all conditions, participants played 30 rounds of an auction game with a randomly assigned single competitor (another participant) on each trial. The range of V was 0 to 100 experimental dollars. In each round, participants knew their own assigned V and the distribution (*28*) of their competitor's assigned values and were asked to submit a bid (b). The participant submitting the highest b won the good. The payoff was equal to V minus b for the winner and zero for the loser.

There were three experimental groups: baseline, loss-frame, and bonus-frame. The baseline condition was a typical first-price auction as described above. The loss-frame auction was identical to the baseline except that participants were given a sum of 15 experimental dollars at the beginning of each round and were told it was theirs to keep if they won the auction, but that they would have to give it back if they lost. As previously discussed, the purpose of the loss-frame was to prime or enhance the possibility of a loss while hypothesizing, based on the observed striatum BOLD responses, that such priming would increase bidding behavior. The bonus-frame auction was again identical to the baseline, except that participants were told that, in addition to receiving the payoff (V minus b), if they won the auction, they would also be given a bonus

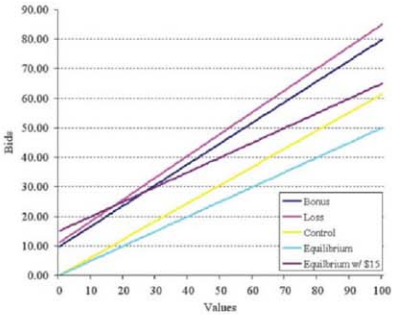

Fig. 2. Estimations of bid functions for the loss-frame, bonus-frame, and baseline control conditions with reference equilibrium functions. Relative to reference equilibrium bids (light blue and purple lines), participants overbid in all three treatment conditions. Consistent with increased overbidding in the loss-frame condition (pink line), bids were higher overall in this condition and the slope of the bidding function was significantly steeper in the loss treatment than in either the bonus-frame (light blue line) ($t = 3.023$, $P < 0.005$) or the baseline control (yellow line) ($t = 11.743$, $P < 0.005$) conditions. In addition, the slope of the bidding function for the bonus-frame condition was significantly steeper than the baseline control condition ($t = 8.283$, $P < 0.005$). See Table 2 for bid functions.

Table 2. Reference equilibrium and estimation of bid strategies for baseline, bonus- and loss-frame conditions. Regressions were conducted with random effects. For estimation of bid strategies, we used a linear specification. Bid functions were estimated using higher-order polynomials, but the coefficients associated with those higher order terms were insignificant.

Condition	Bid function	N	R^2
Equilibrium baseline	$b = 0 + 0.5V$		
Equilibrium + $15	$b = 15 + 0.5V$		
Baseline	$b = 0 + (0.614 \pm 0.011)V$	660	0.805
Bonus-frame	$b = (9.74 \pm 2.547) + (0.702 \pm 0.017)V$	1380	0.733
Loss-frame	$b = (11.09 \pm 2.09) + (0.74 \pm 0.017)V$	1560	0.761

Table 3. Mean revenue by treatment and statistical comparisons (one-tailed t test) of revenues across treatments in the behavioral study. Revenue generated in the loss-frame is significantly greater than both the bonus-frame and baseline conditions. In addition, the bonus-frame condition resulted in greater revenue than the baseline condition.

	Revenue	Analysis	
		Baseline	Bonus treatment
Loss treatment	45.62 ± 1.524	$t(1108) = 3.534$ $P = 0.0002$	$t(1468) = 2.943$ $P = 0.0017$
Bonus treatment	42.41 ± 1.495	$t(1018) = -1.26$ $P = 0.1165$	
Baseline	40.88 ± 1.857		

of 15 experimental dollars. Note that in both the loss- and bonus-frame conditions, only the winners get an additional 15 experimental dollars, so the auctions are strategically identical. The difference is simply the way it is framed (*9*). Given this, equilibrium bid functions are the same in the loss-frame and bonus-frame treatments for any given form of the utility function. In the risk-neutral Nash equilibrium for the two nonbaseline treatments, participants' bids should be the same as the baseline condition plus 15 experimental dollars. However, if the hypothesis derived from our fMRI results is correct and the fear of losing is prompting overbidding, we should observe higher overall bids in the loss-frame condition than either the bonus-frame or baseline conditions.

The bid function for each condition is summarized in Table 2. As expected from previous research, there was overbidding in all three conditions relative to the risk-neutral Nash equilibrium. In addition, there was a constant relative increase in overall bid amount in the two nonbaseline conditions due to the additional potential profit of 15 experimental dollars. Consistent with our hypothesis, there was also a significant difference in the slope of the bid functions across conditions. As can be seen in Fig. 2, the bid function for the loss-frame condition is higher overall than the bid function in all other conditions. This is true despite the fact that both the bonus- and loss-frame conditions have identical equilibrium bid functions. If we calculate the actual revenue to a hypothetical auctioneer generated in the experiment, the revenue generated by the loss-frame (45.62) was significantly higher than either the bonus-frame (42.41) or baseline (40.88) conditions (Table 3). By taking advantage of our knowledge of the brain's reward circuitry, we were able to design a novel auction paradigm that led to greater overbidding.

Previous economic investigations of experimental auctions have led to two opposing views as to the nature of overbidding (*5*, *6*). The combination of neuroscience and behavioral techniques provides an interesting perspective on this age-old question. Both our brain imaging and behavioral results are inconsistent with the suggestion that the "joy of winning" mediates overbidding. Although our findings are not inconsistent with a role for risk aversion in the tendency to bid too high, they suggest we should more specifically consider the fear of losing or social loss aversion. If sensitivity to risk alone is mediating overbidding, then the simple framing manipulation in our behavioral study would not have been effective, because risk was equivalent in both the loss- and bonus-frame conditions. By emphasizing the potential loss in the loss-frame auction, we were able to increase overbidding. Our results suggest that contemplated loss is an important factor in experimental auctions. The fear of losing the social competition inherent in an auction may lead people to pay too high a price for the good for sale. The results of this report, therefore, highlight an extra component in subject's behavior, chiefly the social component of competition, which is not captured by models limited to typical economic variables like profits and probabilities.

Recently, there has been significant debate about whether neuroscience techniques can provide novel insights to economic questions (*1*–*4*). Although there have been a number of neuroeconomics studies that have utilized economic games to further our understanding of brain function, the benefits to traditional behavioral economics as a result is unclear. As was observed in the progression of cognitive neuroscience, using neuroscience models to inform behavioral or psychological questions requires an initial basic understanding of the neural mechanisms underlying the behavior in question (*3*, *4*, *29*). Because of recent advances in neuroeconomics and our knowledge of the neural circuitry of reward, we were able to leverage our neuroimaging results to develop an auction design that highlights the importance of framing and, specifically, the contemplated loss, as an explanation for overbidding during experimental auctions. Our results provide evidence of how an understanding of the neural systems of economic behavior might inform economic theory.

References and Notes

1. A. Rubinstein, in *Advances in Economics and Econometrics: Theory and Applications, Ninth World Congress*, R. Blundell, W. K. Newey, T. Persson, Eds. (Econometric Society 41, Cambridge Univ. Press, Cambridge, vol. 2, 2006), pp. 246–254.
2. F. Gul, W. Pesendorfer, in *Handbook of Economic Methodology*, A. Caplin, A Schotter, Eds. (Oxford Univ. Press, New York, vol. 1, in press).
3. P. W. Glimcher, A. Rustichini, *Science* **306**, 447 (2004).
4. C. F. Camerer, G. Lowenstein, D. Prelec, *J. Econ. Lit.* **43**, 9 (2005).
5. J. C. Cox, B. Roberson, V. Smith, in *Research in Experimental Economics*, vol. 2, V. Smith, Ed. (JAI Press, Greenwich, CT, 1982), pp. 1–43.
6. J. K. Goeree, C. A. Holt, T. R. Palfrey, *J. Econ. Theory* **104**, 247 (2002).
7. R. Cassidy, *Auctions and Auctioneering* (Univ. of Calif. Press, Berkeley, CA, 1967).
8. In auctions, for any given value received, the bidder chooses his optimal bid by trading off the probability of winning (increasing with higher bids) with lower profits if a win occurs. In the trade-off, risk-averse bidders are willing to receive less profit in order to be more certain of a win, hence, overbidding.
9. See supporting online material, available on *Science* Online, for further methodological details including procedures and additional analyses. Each trial was 30 s long, with decisions lasting 4 s, followed by 12 s of fixation and outcomes lasting 2 s, followed by 12 s of intertrial interval.
10. A "loss" refers to losing the bidding phase and not the actual V minus b payoff. There were a few trials where participants' b exceeded the presented V, which resulted in an auction "win" but with an associated cost to this excess overbidding (negative final profit). These trials (six overall, across the experiment) were excluded from neuroimaging analysis.
11. See table S3 and supporting online material (SOM) for further analysis. Overbidding was also significant when the incentive was points [$t(16) = 2.40$, $P < 0.05$].
12. B. Knutson, G. W. Fong, S. M. Bennet, C. M. Adams, D. Hommer, *Neuroimage* **18**, 263 (2003).
13. S. Nieuwenhuis *et al.*, *Neuroimage* **25**, 1302 (2005).
14. M. R. Delgado, L. E. Nystrom, C. Fissell, D. C. Noll, J. A. Fiez, *J. Neurophysiol.* **84**, 3072 (2000).
15. M. R. Delgado, H. M. Locke, V. A. Stenger, J. A. Fiez, *Cogn. Affect. Behav. Neurosci.* **3**, 27 (2003).
16. E. Tricomi, M. R. Delgado, B. D. McCandliss, J. L. McClelland, J. A. Fiez, *J. Cognit. Neurosci.* **18**, 1029 (2006).
17. M. Haruno *et al.*, *J. Neurosci.* **24**, 1660 (2004).
18. J. P. O'Doherty, *Curr. Opin. Neurobiol.* **14**, 769 (2004).
19. Mean beta weights are parameter estimates derived from the general linear model that indicate how much each factor (i.e., individual condition) contributes to the overall data. For detailed explanation see (*30*).
20. Similar results for the left ventral caudate ROI are reported in the SOM.
21. D. J. de Quervain, *Science* **305**, 1254 (2004).
22. E. Fehr, B. Rockenbach, *Curr. Opin. Neurobiol.* **14**, 784 (2004).
23. B. King-Casas *et al.*, *Science* **308**, 78 (2005).
24. P. R. Montague, B. King-Casas, J. D. Cohen, *Annu. Rev. Neurosci.* **29**, 417 (2006).
25. M. R. Delgado, R. H. Frank, E. A. Phelps, *Nat. Neurosci.* **8**, 1611 (2005).
26. R. A. Poldrack, *Trends Cognit. Sci.* **10**, 59 (2006).
27. S. M. Tom, C. R. Fox, C. Trepel, R. A. Poldrack, *Science* **315**, 515 (2007).
28. The distribution of values for all bidders was uniform over the four values available (i.e., each value had an equal probability of being chosen).
29. E. A. Phelps, in *Nature of Cognition*, R. Sternberg, Ed. (MIT Press, Cambridge, MA, 1999), pp. 295–313.
30. S. A. Huettel, A. W. Song, G. McCarthy, *Functional Magnetic Resonance Imaging* (Sinauer Associates, Sunderland, MA, 2004), p. xviii.

31. The authors would like to acknowledge support from the James S. McDonnell Foundation and National Institute of Mental Health, NIH (MH62104) to E.A.P. and the support of the Seaver Foundation to NYU's Center for Brain Imaging. We also thank the Center for Experimental Social Science for its support. We are grateful to D. Schwarz for his efforts in the initial stages of collection and analysis of neuroimaging data. We thank J. Zakrzewski and K. Nearing for their assistance during data collection, M. Nimitkiewicz for assistance during data analysis, and R. Advani for his programming help on the behavioral experiment.

Supporting Online Material

www.sciencemag.org/cgi/content/full/321/5897/1849/DC1
Materials and Methods
SOM Text
Figs. S1 to S3
Tables S1 to S5
References

8 April 2008; accepted 7 August 2008
10.1126/science.1158860

Stirring System

Viscous reaction mixtures often require more powerful stirring than can be achieved with magnetic stirrers. The Vortex stirrer system converts a single overhead stirrer into a powerful three-position parallel stirrer combined with a multiple heating block. The combination of Vortex stirring and DrySyn heating blocks provides efficient stirring while retaining the benefits of the DrySyn range, including safety, rapid heat transfer, and a small size. Used with a standard laboratory hotplate, the unit becomes a compact, small-footprint reaction station capable of running up to three parallel reactions in conventional round-bottom flasks.

Asynt
For information +44-(0)-1638-781709
www.asynt.com

Data Management for Sequencing Platforms

The HT-BLIS productivity system provides an enterprise-scale informatics environment for integrating, analyzing, and sharing data generated by next-generation sequencing systems. HT-BLIS can process, in real time, the massive amounts of data generated by high throughput genomic analysis systems such as Applied Biosystems' Solid System, Helicos's HeliScope Sequencer, Illumina's Genome Analyzer, and Roche's Genome Sequencer FLX System. The latest genomic analysis technologies generate millions of sequences with billions of bases per day. While this capability offers unprecedented resolution and speed for gene expression, sequencing, and genotyping projects, the huge data volumes overwhelm existing informatics infrastructures. HT-BLIS addresses this challenge by receiving, storing, and manipulating in real time the massive amounts of data generated by banks of next-generation sequencers.

Biotique Systems
For information 775-787-9900
www.biotiquesystems.com/HT-BLIS

Handheld X-Ray Fluorescence Instrument

The TracerturboSD is a handheld X-ray fluorescence instrument that features a silicon drift detector (SDD) for dramatically improved speed, sensitivity, and resolution. Bruker's XFlash SDD has been integrated into the handheld device to achieve the speed, analytical specificity, and energy resolution that is generally found only in more expensive laboratory systems. New applications include art conservation, archeology analysis, and the aerospace industry, where users can better analyze light element alloys, even without the use of vacuum or helium attachments.

Bruker AXS
For information 609-847-9468
www.bruker-axs.com

End Repair Kit

The End-It DNA End Repair Kit is for treating fragmented genomic DNA for use in next-generation DNA sequencing. The kit converts DNA containing damaged ends, 5' protruding ends, or 3' protruding ends to 5'-phosphorylated, blunt-ended DNA for fast and efficient ligation to sequencing adapters. The end-repaired, 5'-phosphorylated DNA can then be efficiently ligated using Epicentre's Fast-Link DNA Ligation Kit.

Epicentre Biotechnologies
For information 800-284-8474
www.EpiBio.com

Electrochemical Detection Guide

ESA Electrochemical Detection Guide is a 14-page brochure that leads the reader through the features, benefits, and technical specifications of high-performance electrochemical detectors. It describes systems optimized for applications ranging from identifying oxidation or metabolic products of small molecules to making fast measurements of neurotransmitters in discrete brain regions. These systems offer a wide range of detection options, advanced amperometric and coulometric cells, pumps that minimize background noise, data stations, and high-precision autosamplers.

ESA Biosciences
For information +44-1844-239381
www.esainc.com

Freeze Drying System

The Virtis Genesis Freeze Drying System offers the versatility for use in pilot, research, and small-scale applications. The compact, freestanding, mobile design enables the system to be optimally configured to almost any freeze drying application. New ergonomic profiling allows easy inspection of the vacuum pump and facilitates quick, trouble-free oil changes. A clean room version is also available. The product chamber, shelves, and condenser chamber are made of durable stainless steel, with a squared product chamber that ensures easy cleaning and maximum shelf area. A four-inch diameter port increases vapor flow from the product to the condenser chamber, maximizing productivity. It is available with up to six bulk-drying shelves and five vial processing shelves.

Genevac
For information +44-1473-240000
www.genevac.com

Electronically submit your new product description or product literature information! Go to **www.sciencemag.org/products/newproducts.dtl** for more information.

Newly offered instrumentation, apparatus, and laboratory materials of interest to researchers in all disciplines in academic, industrial, and governmental organizations are featured in this space. Emphasis is given to purpose, chief characteristics, and availability of products and materials. Endorsement by *Science* or AAAS of any products or materials mentioned is not implied. Additional information may be obtained from the manufacturer or supplier.

FRENCH RESEARCH IN TRANSITION

More funding, more autonomy and a new administrative system: over the past three years, French scientific research has undergone massive reforms. From the establishment of the National Research Agency (*Agence Nationale de la Recherche*, ANR) in February 2005 to new laws on research and university autonomy passed in April 2006 and August 2007, France is now on a road to modernization which aims both to simplify and rejuvenate what President Nicolas Sarkozy described last March as "an old moth-eaten system *(un vieux statut mité)*." **By Michel Leroy, Laurent Passicousset, and Julie Clayton**

Until now, research in France has been divided among five different types of organizations: universities, elite higher education institutions (the *grandes écoles*), national research agencies such as the National Center for Scientific Research (*Centre National de la Recherche Scientifique*, CNRS), foundations such as the Pasteur Institute, and private labs. The reforms are shaking up research mainly in the public system, to enhance collaboration and international competitiveness, pay structures, and recruitment of foreign scientists.

Among the 360,000 researchers in France today, 55 percent work for the private sector, mainly in four industrial fields: electronics, engineering, computer services, and pharmaceuticals. The public sector, meanwhile, struggles to attract the best new researchers, competing both with the private sector and with international labs. To make matters worse, most of the alumni from the science and engineering *grandes écoles* do not move on to graduate training, preferring management positions in industry to a research career. And research priorities are different, as public funding focuses on life sciences, social sciences, math/physics/chemistry, and space exploration.

> "The reforms are shaking up research mainly in the public system, to enhance collaboration and international competitiveness, pay structures, and recruitment of foreign scientists."

More Collaboration, More Funding

One of the most significant measures of the French reforms is the law called Freedom and Responsibilities of the Universities (also known as the Autonomization Law), which was adopted three months after Sarkozy's election. This gives university presidents more freedom to recruit staff, manage their assets and budgets, create partnerships with industry, and look for additional funding from private companies.

A key goal of this and other reforms is to enhance collaboration between different players, including with industry, even though 90 percent of the CNRS's 1,200 departments are already joint bodies, or units, comprising university and research agency laboratories.

Public-private partnership is also encouraged as a way to attract both new funding and industry collaboration, inspired by the so-called American R&D model of a more industry-oriented approach.

"We need to be clear," says **Gérard Posa,** director general of the newly established Lyon 1 University Foundation. "France's culture does not allow us to be copycats of the American system. Nevertheless, we have chosen the closest model we could, with clear aims and ways to achieve them: a system that works like industry does."

Eighteen years ago, Posa established, alongside Lyon 1, a commercial body called Ezus. Ezus brings together leading chemical and biopharmaceutical companies to invest in applied research in this city, France's second continued »

"There's no rivalry between those who want to work in state-funded research and those who want to work in the private sector."
—Jacques Berger

largest. The venture has doubled its turnover in the past five years to €14 million ($20.2 million), and has filed several dozen patents. According to Posa, "The aim of a foundation is to work as a facilitator on a noncommercial basis. Our strength is to be on the ground. We know intimately each department and each laboratory of our university—and thus their potential."

Despite Lyon 1 University moving slowly initially, the collaboration with Ezus has paved the way for cultural change, creating a far closer relationship and collaboration with industry.

Other institutes have followed the trend, such as the National Institute for Agricultural Research *(Institut National de la Recherche Agronomique,* INRA), which enjoyed a turnover of €8.2 million ($11.8 million) in 2007 and an 8 percent rise from the previous year in industry-funded research.

Competitiveness

Under the 2007 law, French universities can establish foundations for receiving donations. The foundations can then determine which research projects, facilities, or positions they wish to support, including the appointment of new chairs and the provision of competitive salaries to attract prominent researchers. "A survey identified foreign research workers who would be interested in coming to Lyon," Posa says. "Within the next year, at least two or three new chairs will be established to welcome them."

One of the Lyon-based investors is vaccine manufacturer Sanofi Pasteur, whose president, **Jacques Berger,** sees many benefits to the changes: "There's no rivalry between those who want to work in state-funded research and those who want to work in the private sector," he says. As a result, Berger has witnessed closer cooperation between university and industry researchers, particularly in areas where university researchers excel.

In the awarding of their funding, the foundations, like the universities, are giving priority to global competitiveness clusters identified by the government in 2005. The LyonBioPole is one of these, dedicated to virology, immunology, and diagnostics.

In mid July, the ministry selected all but one of the 10 campuses that will be revamped with such a global perspective in mind. These constitute the pilot group of a €5 billion ($7.2 billion) renovation plan, achieved through the amalgamation of universities. The universities, rather than the ministry, decide upon their involvement—an illustration of their new autonomy. For the first time, the French egalitarian system has been abandoned: the project encompasses just 39 out of the 83 existing universities.

The first nine pilot campuses are in Bordeaux, Grenoble, Lyon, Montpellier, Strasbourg, Toulouse, Aubervilliers, Aix-Marseille, and Saclay, the last being a huge and frequently postponed project, once described as a French MIT, 20 km south of Paris. The tenth, somewhere in central Paris, will be announced in November. This list also illustrates another aspect of the French reforms—a greater devolution of power to the regions. The regions seeing the highest investment are Ile-de-France (Paris), Rhône-Alpes (Lyon, Grenoble) and Aquitaine (Bordeaux). Trailing behind are Auvergne (Clermont-Ferrand) and Alsace (Strasbourg).

Not everyone is convinced, however, that the changes will lead to better results. An American astrophysicist, **David A. Smith,** moved to France 15 years ago after a stopover in Pisa, Italy. He now works for the Nuclear Studies Center *(Centre d'Etudes Nucléaires)* in the southwest city of Bordeaux, in a CNRS laboratory.

"In the USA, everybody cooperates and exchanges. This is part of a long-lasting tradition. Here in France, everything is fragmented," he laments. "I support the desire to make people work together, but administrative grouping does not automatically lead to collaborative groups of people."

Many in the scientific community point out that they did not wait for the latest reforms before applying for funds and developing collaborative projects. "Despite having some deficit in applied science, some projects already exist," says **Jean Esterle,** a professor at Bordeaux 1 University. "Last January, we launched a research study with the National Institute for Research in Computer Science and Control *(Institut National de Recherche en Informatique et en Automatique,* INRIA), together with the neighboring Pau University and various partners including the oil company, Total."

Furthermore, France was the third largest beneficiary of the European Union's 6th Framework Programme for Research and Technological Development, winning a 13 percent share of the overall sum available, i.e., €2.17 billion ($3.13 billion). This has helped enhance the country's ability to compete in the international arena and attract foreign talent.

According to Esterle, the scientific community in Bordeaux is already internationalized. "We have among our permanent staff mathematicians from Germany, Russia, Bulgaria, the United States, China, and Iran."

Nationally, 20 percent of the Ph.D. candidates come from outside the European Union. But the number of foreign postdoctoral scientists is dramatically lower. To redress this, the 2008 state budget has increased by 10 percent the funds aimed specifically at allowing universities to attract postdocs.

The new trend toward increasing employment of scientists from abroad is already evident in the universities, where 10 percent of newly appointed associate professors and 15 percent of full professors now come from abroad.

Attracting Talent

A major attraction for foreign researchers is that the French national research agencies and universities employ researchers on permanent civil service contracts. "Probably the most crucial step at the beginning of a career is to secure civil servant status," says Smith of the Nuclear Studies Center. "It gives peace of mind and the ability to concentrate on one's research."

One research center that is actively recruiting foreign scientists—into biology, ecology, environmental science, and other areas—is INRA, where around 25 percent of candidates for permanent positions are foreigners. INRA is Europe's largest agricultural research center, or rather collection of centers located throughout France. Civil servant salaries are given to those in permanent positions, while overheads are provided for those on short-term contracts. Individual research units seek grants from various sources, including ANR, the EU, private companies, and government ministries. To add to the international flavor, most of the French researchers hired into permanent positions have worked abroad, according to **Thierry Boujard** of INRA's human resources department. "It's really important that our researchers think international, and have an international network."

> "It's really important that our researchers think international, and have an international network."
> —Thierry Boujard

Two years ago INRA also launched a new scheme of providing four-year contracts to foreign researchers who propose their own program of study, with salaries that are higher than those for civil servants. They are then expected to move on to positions elsewhere, but stay part of a collaborative network. "We expect that it will open collaborations for much more than the four years," says Boujard. The institute also takes special steps to help newcomers settle in, organizing accommodation and social security, and providing intensive French language courses.

Starting Out

A prevailing concern in France is the difficulty that early career scientists have in achieving independence in a hierarchical system dominated by experienced heads of labs and departments, particularly in the universities. Most scientists starting out join an existing lab, rather than running their own as is common in the United States and United Kingdom. This is where private foundation–based research centers such as the Paris-based Institut Curie have an advantage, according to director **Daniel Louvard.** On the flip side, French scientists start their career earlier than their US or UK counterparts, due in part to the extended postdoctoral training required in the latter countries.

Institut Curie combines a research center and hospital focusing on the diagnosis and treatment of cancer, and specializing in breast and gynecologic cancers, and pediatric tumors. Its ranks will soon swell from 900 to over 1,000 people with the opening of a new Department of Developmental Biology in October. Six teams are already in place, and the recruitment drive is under way to complete the teams for the opening. Louvard is aiming to hire mostly junior investigators. "We want to stimulate research by giving a chance to young investigators starting either from an existing small group or from scratch, i.e., just finishing their first or second postdoc."

Louvard is also imposing limits on team size. "We want to avoid the formation of big empires and stimulate the interactions between these groups—there's an incentive to collaborate because you're not big enough." In this way, Louvard believes the institute will gain most from its mix of research disciplines and potential for translational research, involving anything from theoretical physics and pharmacochemistry through cell biology and radiobiology to imaging and bioinformatics.

The public system is still "too complicated, too centralized, and too slow," Louvard asserts. In contrast, "Our attractiveness is our ability to react quickly, to be adaptable," including for the employment of foreign researchers. "A postdoc candidate can send me a CV at any time during the year, and continued »

Featured Participants

Bordeaux 1 University
www.u-bordeaux1.fr (in French)

Ezus
www.ezus-lyon.fr (in French)

Institut Curie
www.curie.fr/index.cfm/lang/_gb.htm

Le Havre University
www.univ-lehavre.fr/internat

Lyon 1 University Foundation
www.lyon1fondation.org (in French)

National Center for Scientific Research (Centre National de la Recherche Scientifique, CNRS)
www.cnrs.fr/index.html

National Institute for Agricultural Research (Institut National de Recherche Agronomique, INRA)
www.international.inra.fr

National Institute for Health and Medical Research (Institut National de la Santé et de la Recherche Médicale, INSERM)
www.inserm.fr/en/index.html

National Institute for Research in Computer Science and Control (Institut National de Recherche en Informatique et en Automatique, INRIA)
www.inria.fr/index.en.html

National Research Agency (Agence Nationale de la Recherche, ANR)
www.agence-nationale-recherche.fr/Intl

Nuclear Studies Center (Centre d'Etudes Nucléaires de Bordeaux Grandignan, CENBG)
www.cenbg.in2p3.fr (in French)

Sanofi Pasteur
www.sanofipasteur.com

Young Researchers Confederation (Confédération des Jeunes Chercheurs, CJC)
cjc.jeunes-chercheurs.org (in French)

Focus on France

within two weeks I can say yes or no—granting the possibility of bringing that person in the next day and guaranteeing a 12-month salary equivalent to a Marie Curie Fellowship." He is also providing up to 30 percent extra in salary to scientists who do additional activities such as teaching, training, and interacting with clinicians or with industry.

It is perhaps a testament to this flexibility that the institute has had over 500 postdocs in the past five years, representing almost 50 nationalities, "which makes good lab parties where everybody brings the traditional food of their countries," laughs Louvard. Joking aside, he believes that it is this level of international recruitment that has enabled the institute to achieve "real visibility in biomedical research."

"We are demanding a true doctoral contract, a three-year job contract."
—Morgane Gorria

Retaining Talent

Meanwhile, at the national research agencies, some relatively recent initiatives are giving promising early career researchers their own funds and lab space, to foster their independence.

A 35-year-old specialist in molecular biology, **Fabrice Lejeune,** benefits from an *Avenir* grant from the National Institute for Health and Medical Research (*Institut National de la Santé et de la Recherche Médicale,* INSERM). Over five years Lejeune, a newly tenured scientist, gets €60,000 ($86,400) a year to pay for one postdoctoral fellow and to buy research equipment for the joint INSERM-Pasteur Institute unit in Lille, in northern France where he works. "But I still have to apply for additional funding from the ANR, and to patients' associations like the French Muscular Dystrophy Association," Lejeune explains.

Through the *Avenir* initiative—a program started in 2001 but the effects of which are only now being felt—INSERM awards 20 grants to tenured early career scientists and 20 to nontenured ones. The competition is tough and applicants must have demonstrated academic excellence and capacity for autonomous research.

Lejeune did his Ph.D. in one of France's leading research centers, the Institute of Genetics and Molecular and Cellular Biology (IGBMC), near Strasbourg, eastern France. Following a three year postdoc at the University of Rochester in the United States with professor Lynn Marquat, Lejeune was recruited by INSERM in 2005.

"I chose to come back to France in spite of the salary gap," Lejeune explains. "After three years as a permanent researcher, I have now reached the same salary I had in the United States at the end of my postdoc. This question of low salaries remains difficult even now with my *Avenir* program. I have hired a postdoc from Poland who has to accept the job for a gross salary of €20,400 [around $29,400] a year instead of $40,000 in the States where living costs are lower." And even if Lejeune gets more funding for a postdoc, he will still have to follow the same salary scale at INSERM.

Fair Compensation

The salary issue remains a challenge in France, and is even more sensitive for people just starting on the academic ladder. The *Confédération des Jeunes Chercheurs* (Young Researchers' Confederation, CJC), an umbrella organization of 35 scientists' associations, proposes that Ph.D. candidates should be recognized more as professionals rather than regarded simply as students.

"We are demanding a true doctoral contract, a three-year job contract," says its president, **Morgane Gorria,** an agronomist who has a Ph.D. in biology and currently works as a nontenured assistant professor in Le Havre University in northwestern France. "It is a funding issue and also a way to be recognized by one's peers."

Until now there has been no single type of contract for a Ph.D.—candidates entering doctoral programs must apply for an *allocation de recherche* (research allowance): a monthly salary of around €1,658.25 (about $2,400) paid by the government for up to three years.

Another approach is to join industry through a *Convention Industrielle de Formation par la Recherche* (CIFRE), a private contract partly funded by the government, but which is negotiated with the employer. The average yearly salary is €24,800 ($35,700). Despite the announcement of an increasing number of private-funded contracts, those in the CIFRE program remain in the minority: there are currently 70,400 Ph.D. candidates in France, but only 15,000 contracts have resulted from the launch of the CIFRE program since 1981.

The most common type of funding, however, is the *libéralités* which consist of grants from various bodies and universities, but do not include the benefits of a pension or medical insurance that would be provided by a contract. These are supposed to have been phased out (from 2004 onward), but they still exist for many researchers. The most controversial issue, however, is the change in rules on how scientists are recruited and assessed. According to the new law, universities will have the power to recruit researchers and professors on a short-term basis, although the proportion is still unknown. Moreover, the recruitment procedure has been changed to fight a long-denounced systemic favoritism. From this September, the first universities will implement the new rule that 50 percent of any ad hoc recruitment committee must comprise external members—another key step in a new era for science careers in France.

France's road to modernization of research may not be smooth, and it may be a while before the new funding and autonomy of the universities leads to greater international competitiveness, but it is clear among the scientific community that a shake-up was sorely needed in the old system. Now at least, the reforms do appear to be taking French science in the right direction.

Michel Leroy and Laurent Passicousset are freelance journalists in Paris, France. Julie Clayton is a freelance science journalist based in Bristol, UK.

DOI: 10.1126/science.opms.r0800060